Development of Molybdenum Isotopes as Petroleum Tracers: The Phosphoria Petroleum System, Bighorn Basin, U.S.A.

by

Su Wang

A thesis
presented to the University of Waterloo
in fulfillment of the
thesis requirement for the degree of
Master of Science
in
Earth Sciences

Waterloo, Ontario, Canada, 2018

Authors Declaration

I hereby declare that I am the sole author of this thesis. This is a true copy of the thesis, including any required final revisions, as accepted by my examiners.

I understand that my thesis may be made electronically available to the public.

Abstract

The application of Mo isotope compositions in petroleum systems is a new field of research. In this study, elemental concentrations and Mo isotope compositions were measured on crude oils, asphaltenes separated from the crude oils, and black shale source rocks (Meade Peak Member and Retort Member of the Permian Phosphoria Formation) from the Phosphoria petroleum system, U.S.A. An improved analytical methodology was developed for precise and accurate measurement of the Mo isotope composition of oil and asphaltene samples.

Based on the concentrations of Mo, V, and Ni, the Meade Peak Member and Retort Member shales were deposited in both euxinic and non-euxinic environments. The Mo/TOC and Mo/U ratios of the euxinic shales suggests that the Meade Peak Member was deposited in a weakly to moderately restricted basin whereas the Retort Member was deposited at a time of greater basin restriction.

Crude oils have Mo concentrations of 0.005-0.392 ppm, whereas Mo concentrations in the black shale source rocks reach hundreds of ppm. Hence, the amount of Mo transferred from kerogen in the black shales to the generated oil was low. Asphaltene Mo concentrations are 0.973-3.16 ppm, which are higher than the concentrations of these metals in the bulk crude oils. Hence, asphaltene is a major host of Mo in the Phosphoria crude oils. However, there is no strong correlation between the crude oil and asphaltene concentrations for each metal, suggesting other important hosts for these metals in the maltene fraction of the Phosphoria oils.

The Mo isotope compositions ($\delta^{98/95}$Mo relative to NIST SRM 3134 = 0.25‰) and Mo concentrations in the Phosphoria crude oils, asphaltenes, and source rocks were measured. Asphaltene fractions (0.78-1.44‰) have similar or slightly lower δ^{98}Mo compared with their

bulk crude oils (0.87-1.53‰). Hence, there may be other fractions of the oil that have a higher δ^{98}Mo than the bulk oil and asphaltene. The δ^{98}Mo in crude oils minimally altered by reservoir processes (1.05-1.31‰) are lower than those of the most Mo- and TOC-rich black shales (1.05-1.98‰), implying Mo isotope fractionation during oil generation and/or migration. This observation suggests Mo isotopes are not useful as an oil-source rock correlation tool.

The effect of reservoir processes on the Mo isotope compositions of crude oils in the Phosphoria petroleum system was also evaluated through comparison of altered versus non-altered oils. Crude oils affected by biodegradation and water washing (0.92-1.53‰) do not have significantly different δ^{98}Mo compared to unaltered crude oils (1.05-1.31‰). Crude oils affected by thermochemical sulfate reduction (TSR) have generally lower δ^{98}Mo (0.53-1.23‰) than those in unaltered crude oils. An inverse correlation is observed between the Mo and S isotope composition of the crude oils. The lower Mo isotope composition and higher S isotope composition of TSR-altered oils may have been caused by the introduction of external fluids containing isotopically light Mo and isotopically heavy S into the oil reservoir.

The global ocean redox conditions at the time of Phosphoria Formation deposition can be inferred from the δ^{98}Mo of the euxinic shales. Given that any expression of Mo isotope fractionation between the water column and euxinic sediments results in preferential removal of lighter Mo isotopes to the sediments, the highest δ^{98}Mo values of 1.77‰ and 1.98‰ from the euxinic Meade Peak Member and Retort Member, respectively, represent minimum δ^{98}Mo values for coeval global seawater. These values are consistent with recent Mo and U isotope studies that suggest an extensively oxygenated global ocean in the ~ 18 Myr before the largest Phanerozoic mass extinction event in the latest Permian.

Acknowledgements

I want to express my thanks to my supervisor, Dr. Brian Kendall, for his expert advice and encouragement throughout this project. Without him, I would not have the opportunity to take samples from the United States Geological Survey (USGS) and do experiments at the Metal Isotope Geochemistry Laboratory, Department of Earth and Environmental Sciences, University of Waterloo. The project results cannot be obtained without his assistance and guidance on sample analysis and thesis writing. He always shows the kindness and patience to help his students.

I would like to thank our lab manager, Liyan Xing, for her guidance and kindness when I was doing my lab work. She helped me a lot to complete my lab work procedures.

Dr. Gwyneth Gordon and Dr. Wang Zheng of Arizona State University are thanked for assistance with Mo isotope measurements. The staff of the Agriculture and Food Laboratory, University of Guelph, are thanked for assistance with total organic carbon analyses.

I would like to thank my committee members Prof. Martin Ross and Prof. Shaun Frape for their generous time, constructive advice, and support that have helped me to improve my thesis project. Prof. Shoufa Lin is thanked for reviewing my MSc thesis proposal.

I would like to thank my collaborator Paul Lillis from the USGS. He collected and sent me black shale, oil, and asphaltene samples that gave us the opportunity to do this project.

I would also like to thank the following colleagues, school mates, and friends, for their love and support (including but not limited to): Xinze Lu, Ryan Truong, Jieying Wang, Shuai Yang, Kai Liu, Bingjie Shi, Wei Du, Yiming Cai, Yan Zhang, and Shengliang Lu.

I would like to thank my parents for their support and encouragement during my graduate research.

This study was funded by a NSERC Discovery grant (RGPIN-435930) to Dr. Brian Kendall.

Table of Contents

List of Figures

List of Tables

1. Introduction

1.1. Research Motivation: Application of metal stable isotopes to petroleum systems

Metal stable isotope systems have potential as process tracers and exploration tools for mineral and energy resources (Larson et al., 2003; Mason et al., 2005; Ventura et al., 2015; Swainson, 2017; Kendall et al., 2017). Studies have mainly focused on mineral deposits, particularly Cu, Zn, Mo, and U isotope variations in ore-forming systems (see recent reviews by Andersen et al., 2017; Kendall et al., 2017; Moynier et al., 2017). Although metal isotopes have been used to study the characteristics of petroleum source rocks and their depositional environments (e.g., local and global ocean redox conditions; see the recent review by Kendall et al., 2017, for Mo), few studies have carried out metal isotope analysis of crude oils (Ventura et al., 2015).

Previous research has shown that V and Ni are the most abundant trace metals in oil (Manning and Gize, 1993; Archer et al., 2012). The V and Ni concentrations in oil can be influenced by the depositional environment of the source rock, oil and source rock composition, and the oil migration pathways (Barwise, 1990; Filby, 1994). Measurement of the V isotope composition of geological materials is challenging because more than 99% of V is made up of just one isotope (^{51}V), and method development for V isotope analysis is still emerging (Wu et al., 2016). By contrast, Ni isotope compositions for geological materials are more routinely measured. Archer et al. (2012) reported in a conference abstract that petroleum maturity affects the Ni isotope composition of crude oil. If correct, then Ni isotopes may be more useful as a tracer of reservoir processes and migration pathways than as an oil-source correlation tool.

Ventura et al. (2015) studied crude oil samples sourced from the Campos Basin in Brazil and observed a correlation between V and Ni isotope composition, and V/(V + Ni) ratio, which is a widely used indicator of redox conditions during deposition of the oil's source rock(s). The Campos Basin oil source rocks were not studied for their elemental and isotope characteristics.

Like V and Ni, Mo is a redox-sensitive element that has elevated concentrations in organic-rich mudrocks (ORM) relative to the upper continental crust (average of ~1.5 ppm; McLennan, 2001) because this trace metal is sequestered into organic matter and sulfide minerals in anoxic marine sediments deposited from anoxic to weakly oxygenated bottom waters, with Mo burial rates highest in euxinic (anoxic and sulfidic) environments (Algeo and Lyons, 2006; Tribovillard et al., 2006; Scott and Lyons, 2012). The Mo concentrations and isotope compositions in ORM are commonly used as a tracer to interpret the local and global ocean redox conditions at the time of ancient ORM deposition (Anbar, 2004; Anbar and Rouxel, 2007; Kendall et al., 2017).

By contrast, the Mo isotope analysis of crude oils and their application to petroleum systems is a new field of study. Only one abstract (Archer et al., 2012) and one published article (Ventura et al., 2015) have presented Mo isotope data for crude oils. If crude oils preserve the Mo isotope signatures of the oil-generating source rocks, then Mo isotopes could be used for oil-source rock correlation. On the other hand, reservoir processes, interaction with waters and rocks along oil migration pathways, or the generation and expulsion of oil may alter the Mo isotope compositions of crude oils from source rock compositions. If so, then Mo isotopes could be used to trace oil migration pathways, and/or reservoir processes such as thermochemical sulfate reduction (TSR), biodegradation, and water washing. It is useful to study the Mo isotope compositions in oil and determine potential applications that would complement traditional

geochemical tracers for oil generation, migration, and reservoir storage such as light stable isotopes, radioactive/radiogenic isotopes, and biomarkers.

Oil and source rock samples from the well-characterized Phosphoria petroleum system of the Bighorn Basin, western U.S.A., will be analyzed. Previous biomarker and geochemical data obtained for these oils provide independent information about secondary petroleum alteration during oil migration and storage in the reservoir (biodegradation, water washing, and thermochemical sulfate reduction), as well as organic sources and thermal maturity information (Lillis and Selby, 2013). Based on biomarker distributions, carbon and sulfur isotope compositions, and elemental concentrations, the oil in the Phosphoria system was interpreted to be primarily derived from the Meade Peak Phosphatic Shale Member and the Retort Phosphatic Shale Member of the Permian Phosphoria Formation (Lillis and Selby, 2013).

In addition to testing the use of Mo isotopes as an oil tracer, the Mo isotope composition of the Phosphoria Formation ORM will shed insight on local and global ocean redox conditions at ca. 270-265 Ma. The Permian Period ended with the greatest mass extinction in Earth's history at ca. 252 Ma, in which 95% of species in marine and terrestrial environments died (Benton et al., 2003; Lehrmann et al., 2003). Redox-sensitive element concentrations and isotope compositions suggest that extensive ocean anoxia is associated with the mass extinction (Kato et al., 2002; Algeo et al., 2010; Wignall et al., 2010; Algeo et al., 2011; Brennecka et al., 2011), but the ocean redox conditions during the preceding Permian interval are not well understood because global ocean redox proxies (such as Mo isotopes) have not been applied to sedimentary rocks deposited at this time.

1.2. Research objectives for this study

The major objective of this study is to better understand Mo isotope behavior and its potential applications to petroleum systems, using the Phosphoria petroleum system, Bighorn Basin, northwestern U.S.A., as the case study. The same oil samples measured in this study for Mo concentrations and isotope compositions were previously analyzed by Lillis and Selby (2013) for Re-Os and S isotope compositions, biomarkers, and oil geochemistry. Organic-rich shales and mudrocks from the Meade Peak Phosphatic Shale Member and the Retort Phosphatic Shale Member, deposited in the Phosphoria Sea, were measured in this study for organic carbon content, elemental concentrations, and Mo isotope compositions to provide geochemical information about the oil source rocks (these rock samples were not analyzed by Lillis and Selby, 2013). Specific research goals of this study are:

1. *Method development for Mo isotope analysis of oils*

Ventura et al. (2015) measured Mo isotope data from bulk crude oil samples, but the precision of the Mo isotope data was on average a factor of three lower relative to the precision typically achievable for Mo isotope analysis of ORM and other rocks. Hence, an improved analytical methodology was developed for precise Mo isotope analysis of crude oils in this study. The Mo isotope composition of separate fractions of crude oil, such as the *n*-heptane insoluble (asphaltene) and *n*-heptane soluble (maltene) fractions, have not yet been measured. This study reports the first Mo isotope measurements of asphaltenes, which are known to represent a significant host of metals in crude oils (Lillis and Selby, 2013).

2. *Initial assessment of whether Mo isotopes can be used for oil-source rock correlation*

To accomplish this objective, a regional set of ORM samples from the Meade Peak Phosphatic Shale Member and the Retort Phosphatic Shale Member with high TOC (total organic carbon) was selected for analysis. Thermally immature and mature ORM (with respect to temperatures necessary for oil generation) would best represent the Mo isotope composition of the source rocks that generated oils in the Phosphoria basin. If the Mo isotope composition of the least altered oils (i.e., least affected by secondary reservoir processes) are similar to the Mo isotope composition of the source rocks, then Mo isotopes may be a potential tracer for oil-source rock correlation. However, if the oil and source rock Mo isotope compositions are different, then isotopic fractionation associated with oil generation, migration, and/or reservoir processes must have altered the oil Mo isotope compositions from the starting source rock values.

3. *Evaluate the effect of different reservoir processes on the Mo isotope compositions of oils*

The Mo isotope data from the oils will be compared with known inorganic and organic geochemical indicators of biodegradation (based on gas chromatograms of whole oils and saturated and aromatic hydrocarbon fractions), water washing (based on different levels of saturated and aromatic hydrocarbon fractions to distinguish from the effects of biodegradation), and TSR (based on S isotope data) to determine the impact of these reservoir processes on oil Mo isotope systematics. One expected outcome of the study is a better characterization of the effect of reservoir processes on the Mo isotope compositions of oils.

4. *Mo isotope constraints on global ocean redox conditions in the middle to Late Permian*

The largest biotic extinction during the Phanerozoic lasted from the Late Permian to the Early Triassic (Kato et al., 2002; Algeo et al., 2010). Lithology and geochemistry evidence from rocks in the uppermost Permian sections suggest that the Panthalassic ocean (which comprised 85-90% of the contemporaneous global ocean) shifted to more anoxic and euxinic conditions, particularly along continental margins, during the mass extinction (Kato et al., 2002; Algeo et al., 2010; Wignall et al., 1996; Wignall et al., 2010; Brennecka et al., 2011; Takahashi et al., 2014; Elrick et al., 2017). Geochemical evidence suggests that the global ocean in the 8 Myr (ca. 260-252 Ma) before this oceanic anoxic event had a broadly similar redox state as the modern global ocean (Elrick et al., 2017). Global ocean redox conditions earlier in the Permian Period are not well constrained. Molybdenum isotope analysis of the black shales and mudrocks of the Phosphoria Formation may improve constraints on global ocean redox conditions at ca. 270-265 Ma.

2. Geological Setting

2.1. Geology of the Phosphoria Formation

The Permian Phosphoria Formation was deposited in the Bighorn Basin, and together with its stratigraphic equivalents, covers about 583,000 km^2 in northeastern Nevada, eastern Idaho, southwestern Montana, western Wyoming, northern Utah, and northeastern Colorado (McKelvey et al., 1956; Campbell, 1962). The Phosphoria Formation underlies the Triassic Dinwoody Formation and overlies the Pennsylvanian Tensleep Sandstone Formation (***Figure 1***). The Phosphoria Formation was originally restricted to the phosphatic chert and mudstone facies in southeastern Idaho and adjacent areas (McKelvey et al., 1956; Campbell, 1962; Piper and Link, 2002; Walling, 2010). Subsequently, the Phosphoria Formation was used to represent the carbonate rock facies, red bed facies and phosphatic chert and cherty shale in the Bighorn Basin (Campbell, 1962; Kirschbaum et al., 2007). The carbonate, chert, and siltstone facies thin eastward toward the North American Craton, and become interlayered with the red beds in Goose Egg Formation on the craton (Wardlaw and Collinson, 1986). Two members in the Phosphoria Formation, the Meade Peak Phosphatic Shale Member and the Retort Phosphatic Shale Member, are believed to be the major sources of the oil found in the Bighorn Basin (Claypool et al., 1978).

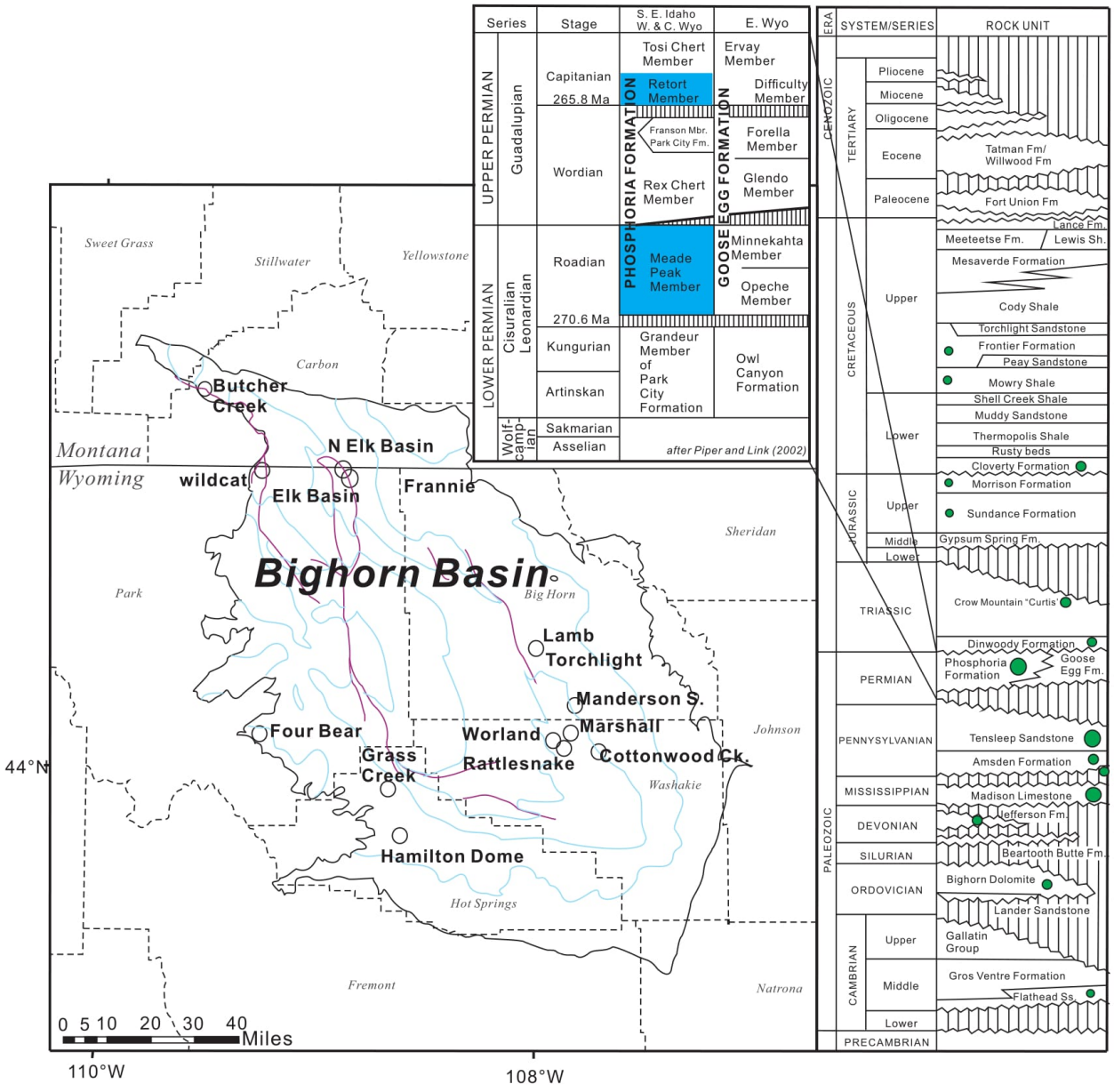

Figure 1. Map of the Bighorn Basin showing the oil sample locations and stratigraphic column for the region. Red lines show faults. Open circles are the oil sample locations. Stratigraphic column shows rock units containing Phosphoria oil (green circles). The sizes of the green circles are proportional to the sizes of the oil fields. Modified from Lillis and Selby (2013).

The Phosphoria Formation was deposited during regressive and transgressive marine cycles in the basin on the western shelf of the North American craton (Maughan, 1994; ***Figure***

2). When the Pangea supercontinent formed, the North American craton moved westward and developed a foreland basin along the western continental margin during the Permian. This basin was partially restricted from the open ocean by an island arc and tectonic highlands, thus promoting the development of anoxic, including euxinic, conditions in the basin (Maughan, 1994; Piper and Link, 2002; Walling, 2010). Geochemical data together with paleoclimate and ocean circulation models for the Phosphoria Sea suggest that an intermediate water mass entering an epicontinental embayment was relatively oxygen-poor and nutrient-rich (Hiatt and Budd, 2003). Seasonal (summer) upwelling circulation as well as inflow of warm waters from shallow lagoons to the east delivered nutrients to the shallow warm waters of the Phosphoria Sea, causing elevated primary productivity (Hiatt and Budd, 2001, 2003). Together with partial basin restriction that slowed the rate of deep-water renewal, the high organic carbon export flux resulted in O_2 depletion via respiration, leading to the deposition of anoxic organic- and phosphate-rich sediments of the Meade Peak Member and Retort Member in the outer and middle portions of a broad ramp (McKelvey et al., 1956; Parrish, 1982, Maughan, 1994; Hiatt and Budd, 2003; Walling, 2010). In these anoxic settings, phosphogenesis is thought to have been triggered by the release of organic-bound phosphorus via organic matter breakdown in the sediments. Anoxic and euxinic conditions are thought to have prevailed in the mid-ramp setting where the inflowing intermediate water mass directly intersected the seafloor in the Phosphoria Sea, whereas deeper-water outer ramp settings were weakly oxygenated to anoxic (Hiatt and Budd, 2003).

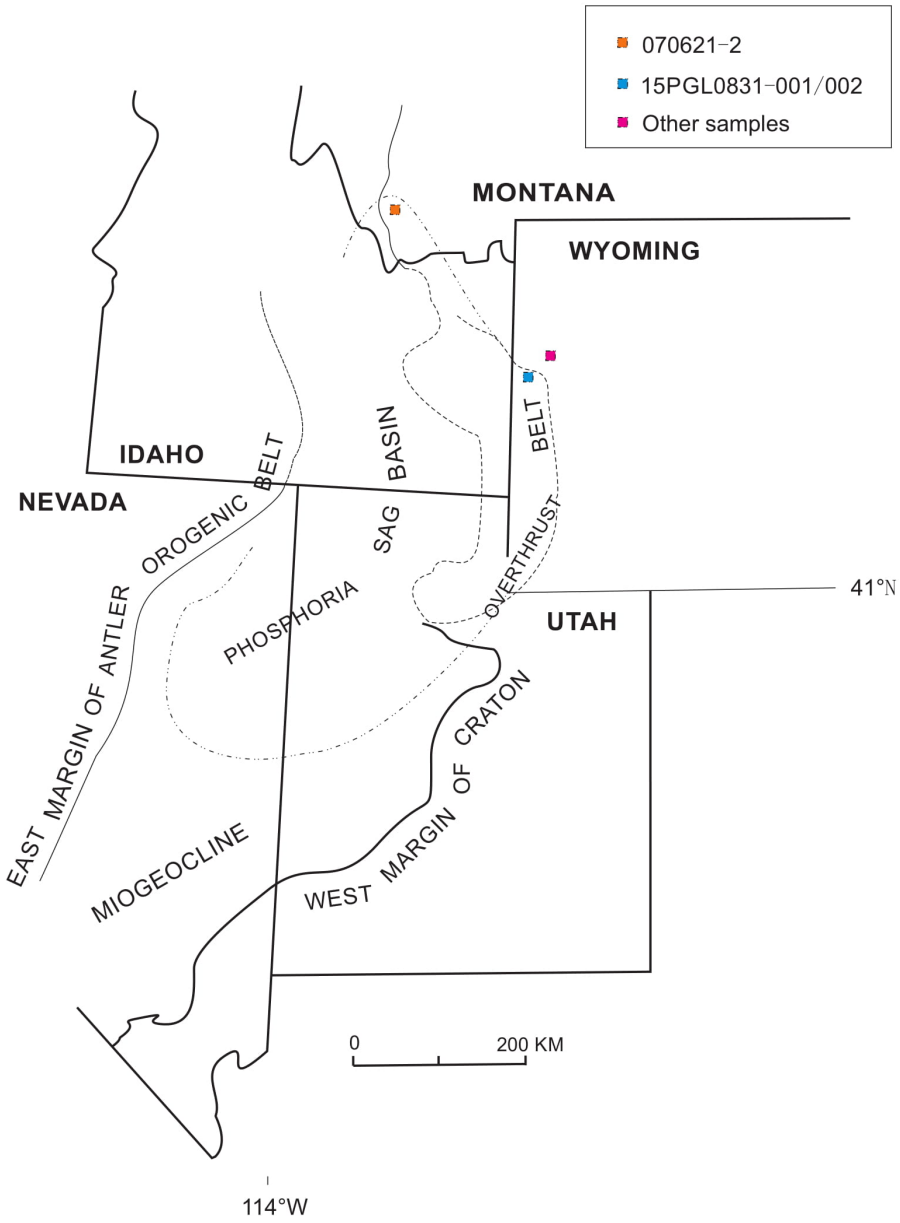

Figure 2. Tectonic setting of the Phosphoria depositional basin (modified from Wardlaw and Collinson et al., 1986). Pink, orange and blue points are the collected black shale sample locations for this study. The dash lines denote the area of the Phosphoria sag basin.

Based on geochronological constraints and biostratigraphic data, the ~60 m thick Meade Peak Member was deposited during the Roadian stage (beginning at ca. 270.6 Ma), whereas the

~30 m thick Retort Member was deposited during the Capitanian stage (beginning at ca. 265.8 Ma; Gradstein et al., 2004; Lillis and Selby, 2013). Although both units are organic-rich oil-prone source rocks (Lillis and Selby, 2013), the Retort Member has generally higher TOC contents (0.6-19.1 wt%) than the Meade Peak Member (0.4-4.2 wt%), as well as higher hydrocarbon contents (Claypool et al., 1978). The oil-generating areas of the Meade Peak and Retort Members are about 118,000 km^2 and 143,000 km^2, respectively (Maughan, 1975). Petroleum derived from the Phosphoria Formation has been found in upper Paleozoic rocks in the central and northern Rocky Mountain region (Claypool et al., 1978; Lillis and Selby, 2013).

Based on kerogen atomic S/C ratios, the Phosphoria Formation source rocks have Type II-S kerogen (Lillis and Selby, 2013). Type II-S kerogen is oil and gas prone and is characterized by moderately high hydrogen and uncommonly high organic sulfur contents. These source rocks would have begun to generate oil at a lower thermal maturity than typical Type II kerogen with low sulfur contents (Dembicki, 2009). The organic source of the Phosphoria oils contained algal and bacterial organic matter dominated by liptinite macerals (Dembicki, 2009). The type II-S kerogen suggests deposition of the source rocks in a marine depositional environment (Dembicki, 2009) where anoxic/euxinic conditions prevailed in the bottom waters and sediments, and reactive iron availability was not sufficient to remove all dissolved hydrogen sulfide as pyrite (Orr, 1986). The burial of Permian strata by Mesozoic sediments led to oil generation in the Phosphoria Basin located in eastern Idaho and western Wyoming (Claypool et al., 1978; Lillis and Selby, 2013). Subsequent overthrusting during Jurassic time also influenced oil generation (Claypool et al., 1978; Edman and Surdam, 1984; Lillis and Selby, 2013). Oils migrated eastward from eastern Idaho and western Wyoming to central Wyoming along regional dip and was trapped in a stratigraphic trap (Campbell, 1962; Lillis and Selby, 2013).

Subsequently, the oil re-migrated and was trapped in structural traps formed by the Laramide orogeny (Campbell, 1962). The generation and migration of oil began sometime in the Late Triassic to Late Cretaceous (Claypool et al., 1978; Lillis and Selby, 2013). In the Bighorn Basin that succeeded the Phosphoria Basin, oil generation ages are suggested to be Paleocene, whereas oil may have been generated during the Late Cretaceous in the adjacent Green River and Wind River Basins located south of the Bighorn Basin (Lillis and Selby, 2013). The Re-Os age of oils not affected by TSR is 211 ± 21 Ma, which is suggested to reflect the beginning of oil generation (which may have lasted > 70 Myr) rather than the source rock age or the oil migration age (Lillis and Selby, 2013).

2.2. Geochemistry of the Phosphoria oils

Molecular biomarkers and light stable isotope systems in oils and their source rocks have been widely used for oil-oil and oil-source rock correlations, estimating the thermal maturity of oils and source rocks, reconstruction of source rock depositional environments, and for developing models of oil generation and migration (Philip, 2004; Peters et al., 2005). However, biomarkers are also influenced by biodegradation, which can destroy the light fractions of oil (Peters et al., 2005). Hence, biomarkers are also commonly used as a tracer for the extent of biodegradation (Peters et al., 2005). In contrast to biomarkers, the hydrogen, carbon, nitrogen, and sulfur isotope compositions in crude oils may not always be affected by biodegradation processes (Marcano et al., 2013). Metals tend to reside in the heavy asphaltene fraction of oil (Filby, 1994; Duyck et al., 2002; Lillis and Selby, 2013), which is more resistant to biodegradation than the light oil fractions. Recently, it was shown that the Re-Os isotope system is not appreciably affected by biodegradation (Lillis and Selby, 2013). Hence, metal isotope

systems may generally not be affected by biodegradation. Similarly, metal isotope systems may also be resistant to water washing because the asphaltene fraction is difficult to dissolve in water (Lillis and Selby, 2013). The S isotope compositions ($\delta^{34}S$) of oils are related to the characteristics of the source kerogen, so it has potential application in oil-source rock correlation (Lillis and Selby, 2013). However, the $\delta^{34}S$ of oils are affected by TSR (Lillis and Selby, 2013). Similarly, TSR is known to significantly alter the Re-Os isotope systematics of oils (Lillis and Selby, 2013). Hence, TSR may affect other redox-sensitive metal isotope systems like Mo.

Some of the Phosphoria oils in the Bighorn Basin have been variably altered by biodegradation, water washing, and TSR (Lillis and Selby, 2013), and hence the effect of these reservoir processes on the Mo isotope composition of oils will be assessed in this study. **Table 1** shows the Phosphoria oil samples that were available to be analyzed in this study and were the focus of a previous Re-Os isotope study by Lillis and Selby (2013).

Biodegradation and water washing are processes that commonly occur together and it is difficult to distinguish their effect on the geochemistry of crude oils (Lillis and Selby, 2013). Gas chromatograms of whole oils and saturated and aromatic hydrocarbon fractions can be used to infer the extent of biodegradation (e.g. **Table 1**; Lillis and Selby, 2013). On the biodegradation scale developed by Peters et al. (2005), level 0 indicates oils have not been affected by biodegradation whereas the maximum level of 10 indicates the greatest extent of biodegradation. Water washing has the potential to remove light aromatic hydrocarbons due to their higher solubility compared with heavy aromatic hydrocarbons and saturated hydrocarbons (Kuo, 1994; Lillis and Selby, 2013). Oil samples are inferred to be affected by water washing if there is a lower abundance of aromatic hydrocarbons than saturated hydrocarbons. As **Table 1** shows, many Phosphoria oil samples are not affected by biodegradation (level 0), whereas the maximum

extent of biodegradation is level 5 based on aromatic hydrocarbons and level 3 based on saturated hydrocarbons (Lillis and Selby, 2013). Those samples with a lower biodegradation level inferred from saturated hydrocarbons compared to aromatic hydrocarbons may reflect water washing of the oil.

Table 1. Sample information for the Phosphoria-sourced oils, Bighorn Basin, U.S.A

Sample	Field Name	Well Name	Formation	Top (ft)[a]	Lat (N)	Long (W)	Biodegradation[b]	GC Comments[c]	Volume available (ml)	Asphaltene name	Asphaltene (g)
1	Butcher Creek	Cruse 1-A	Cloverly (Greybull Mbr. or "Lakota")	260	45.259	-109.533	sats 3 / arom 4	second charge of C_{8-17} n-alkanes	2	33102	0.747
2	Cottonwood Creek	Cottonwood Creek Unit 1	Tensleep	5672	44.065	-107.693	sats 0	no arom GC	0.5	33106	0.018
3	Elk Basin	Unit 193	Bighorn Dolomite	5744	44.970	-108.846	sats 0 / arom 2		0.4	33107	0.015
4	Elk Basin N.	EBMU 32	Madison	5076	44.999	-108.879	sats 0 / arom 0		0.3		
5	Fourbear	Unit 31	Tensleep	3325	44.122	-109.258	sats 2 / arom 5	large UCM	0.2	33104	0.067
6	Frannie	USA PHIL-Rosenburg 27-C	Madison	2925	44.985	-108.636	sats 2 / arom 5	moderate UCM	0.3		
7	Grass Creek	Unit 10-D	Amsden (Darwin Mbr.)	4480	43.944	-108.659	sats 0 / arom 0	elevated phytane/nC_{18}	0.5		
8	Grass Creek	Stateland 50	Cloverly (Greybull Mbr. or "Lakota")	1993	43.943	-108.660	sats 0 / arom 0	elevated phytane/nC_{18}	2	33103	0.273
9	Hamilton Dome	Rathvon 8	Tensleep	2858	43.786	-108.609	sats 0 / arom 0		0.8	33109	0.091
10	Lamb	Lamb 11	Madison	3752	44.404	-107.979	sats 2 / arom 5	moderate UCM	2		
11	Manderson South	State 2	Tensleep	4255	44.214	-107.801	sats 0 / arom 0	high C_{30-40} n-alkanes	2		
12	Marshall	USA Texaco 1	Phosphoria	9706	44.123	-107.824	sats 0 / arom 0		1.5	33105	0.048
13	Rattlesnake	Faure 2A	Phosphoria	10820	44.079	-107.850	sats 0 / arom 0		0.3		
14	Torchlight	TLMTU 42	Phosphoria	3178	44.376	-107.987	sats 1 / arom 0	minor UCM	2		
15	Torchlight	TLMTU 50	Madison	3399	44.376	-107.975	sats 1 / arom 5	minor UCM	2		
16	Torchlight	USA Bel C 1	Madison	3818	44.377	-107.992	sats 2 / arom 5	large UCM	2	33108	0.258
17	Torchlight	Orchard Unit 10	Madison and Bighorn Dolomite	3381	44.378	-107.972	sats 1 / arom 2	minor UCM	0.4		
18	wildcat	O-Hara Fed. 5-24	Phosphoria	11071	44.994	-109.254	sats 1 / arom 0	minor UCM	missing		
19	Worland	Worland Unit 46 M-F-28	Tensleep	10172	44.105	-107.901	sats 0 / arom 0		2		

[a]The depth of well where produced the oil

[b]Biodegradation scale of Peters et al. (2005) based on saturated hydrocarbons (sats) and aromatic hydrocarbons (arom).

[c]GC- gas chromatography; UCM- unresolved complex mixture.

Table modified from Lillis and Selby (2013)

Phosphoria oils typically have low API (American Petroleum Institute) gravity and high asphaltene contents (Bjorøy et al., 1996). API gravity expresses the gravity or density of petroleum products and shows how light or heavy an oil product is compared to water. If oil is lighter and floats on water, its API gravity is greater than 10; if oil is heavier and sinks through water, its API gravity is less than 10. The gravity of oil samples sourced from the Phosphoria Formation ranges from 12.1 to 31.3 °API, and the asphaltene fraction of the oil ranges from 3.1 wt% to 20.3 wt% (**Table 2**).

Table 2. Physical and chemical characteristics of Phosphoria-sourced oils, Bighorn Basin, USA

Sample	Gravity (°API)	Asp (wt%)	TAS	S (wt%)	$\delta^{34}S$ (‰)
1	12.7	8.4	0.10	3.9	-6.2
2	21.6	10.4	0.15	2.7	-4.6
3	24.6	8.4	0.19	1.8	-3.4
4	29.6	4.1	0.18	1.9	-1.2
5	12.1	20.3	0.09	3.6	-5.4
6	16.3	9.0	0.15	3.3	1.7
7	22.5	10.7	0.08	3.0	-4.7
8	22.8	7.9	0.09	2.6	-4.0
9	30.9	11.4	0.15	2.3	-4.7
10	16.7	11.3	0.16	3.0	-0.9
11	31.3	7.2	0.46	1.6	5.7
12	25.9	3.1	0.13	2.8	0.3
13	25.5	6.1	0.17	2.5	1.0
14	22.1	9.5	0.20	2.5	4.1
15	19.4	11.8	0.16	2.6	1.7
16	14.2	15.9	0.17	2.7	1.9
17	21.0	11.7	0.22	2.5	2.8
18	22.1		0.33	2.0	1.0
19	26.2	8.8	0.22	2.2	-4.1

Data from Lillis and Selby (2013)
Asp is asphaltenes
TAS is triaromatic steroid

TSR is an important alteration process in oil reservoirs. The Phosphoria oils have high sulfur contents of 1.6 wt% to 3.9 wt% (**Table 2**). In the TSR process, sulfur is reduced by hydrocarbons, and the hydrocarbons are oxidized inorganically at high temperature (Orr, 1974; Machel, 2001). The minimum temperature is at least 100°C for TSR and depends on oil composition, reservoir conditions, availability of anhydrite (a sulfate source), initial H_2S content in the reservoir environment, and the kinetics of the reaction (Orr, 1974; Gladhaber and Orr, 1995; Worden et al., 1995; Machel, 2001). The main products include sulfide as well as carbon dioxide produced from the oxidation of hydrocarbons (Lillis and Selby, 2013). Other primary and secondary products are solid bitumen, metal sulfide minerals, carbonate minerals, and water (Lillis and Selby, 2013).

The hydrogen sulfide initiates the thermochemical sulfate reduction, and behaves as a catalyst for the reaction (Orr, 1974). According to Orr (1974), Connan and Lacrampe-Couloume (1993), and Worden et al (2000), the two reactions and net reaction are:

a) Sulfate – pre-existing hydrogen sulfide reaction:

Equation (1): $3H_2S + SO_4^{2-} \rightarrow 4S^0 + 2H_2O + 2OH^-$

b) Oxidation of hydrocarbons (the reaction below used the methylene group -CH_2- to represent the hydrocarbons) by elemental sulfur:

Equation (2): $4S^0 + 1.33(CH_2) + 2.66\,H_2O \rightarrow 4H_2S + 1.33\,CO_2$

The net reaction is:

Equation (3): $SO_4^{2-} + 1.33(CH_2) + 0.66H_2O \rightarrow H_2S + 1.33CO_2 + 2OH^-$

In this detailed mechanism for TSR, hydrogen sulfide not only serves as a catalyst but also is a reaction product.

TSR causes high $\delta^{34}S$ values in the Phosphoria oils because the Phosphoria sulfate and evaporites in the Goose Egg Formation are isotopically heavy (Orr, 1974; Lillis and Selby, 2013). The Phosphoria oils that are not affected by TSR have $\delta^{34}S$ values averaging about –4‰, whereas crude oils altered by TSR have $\delta^{34}S$ values up to +8‰ (Orr, 1974; Lillis and Selby, 2013). When the $\delta^{34}S$ values of the Phosphoria oils are greater than –2‰, the oils are considered to be altered by TSR (Lillis and Selby, 2013). The source of the sulfate that causes TSR in the Phosphoria petroleum system is anhydrite in the Phosphoria and equivalent evaporate formations (Goose Egg Formation) (Lillis and Selby, 2013). The Phosphoria oils that have been altered by TSR occur along the eastern edge of the Bighorn Basin where a change in sedimentary facies causes the Phosphoria Formation to transition to the Goose Egg Formation (Campbell, 1962; Lillis and Selby, 2013).

Biomarker ratios and various ratios among aromatic components have been proposed as thermal maturity parameters for oil (Bjorøy et al., 1996). Based on previous research, side-chain cleavage of TASs (triaromatic steroids; formation of C_{20} and C_{21} from $C_{26} – C_{28}$) is the most useful indicator to measure the maturity of oil in the Bighorn Basin (Bjorøy et al., 1996). Based on the ratio $(C_{20} + C_{21})/(C_{20} + C_{21} + C_{26} + C_{27} + C_{28})$, oil maturities are classified as low (< 0.15), normal (0.15-0.32), and high (0.32-0.75) (Bjorøy et al., 1996). Thermal condensates can explain TAS values above 0.75 (Bjorøy et al., 1996). Most of the Phosphoria oil samples have TAS values below 0.3, indicating that the Phosphoria-sourced oils in the Bighorn Basin have normal maturity and that significant thermal cracking did not occur in the reservoir (Lillis and Selby, 2013). Hence, the effect of thermal cracking on the Mo isotope compositions of oils will not be a

focus of this study.

Based on the geochemical characteristics of the Phosphoria oils, the effect of various reservoir processes on oil samples from the Phosphoria petroleum system are summarized in **Table 3**. These sample groupings are used in this study to assess the impact of reservoir processes (TSR, biodegradation, and water washing) on the Mo isotope composition of the Phosphoria oils.

Table 3. Oil samples grouped according to the impact of reservoir processes

Reservoir Effect	Oil Samples
NOT affected by biodegradation + water washing + TSR	2, 7, 8, 9, 19
Affected by TSR	4, 11, 12, 13, 14, 18
Affected by biodegradation + water washing	1, 3, 5, 17
Affected by biodegradation + water washing + TSR	6, 10, 15, 16

3. Background: Molybdenum Geochemistry

Redox-sensitive metal concentrations and isotope compositions (e.g., Mo, U, Fe) in sedimentary rocks such as ORMs can be used for inferring the paleoredox conditions of depositional environments (Neubert et al., 2008; Weyer et al., 2008; Kendall et al., 2011; Asael et al., 2011; Scott and Lyons, 2012; Kendall et al., 2015). Molybdenum is one of the most commonly studied metal isotope systems because of its redox-sensitive nature. The most common Mo oxidation states at typical pH values in aqueous environments are +6 for oxidizing conditions and +4 for reducing conditions. Molybdenum is a conservative element in oxygenated seawater, with a global average concentration of 105 nmol/kg and a long residence time of 440 kyr (Collier, 1985; Miller et al., 2011). High concentrations of Mo are found in anoxic ORMs (to > 100 ppm) compared with the average upper crust (1.5 ppm) (McLennan, 2001; Tribovillard et al., 2006; Scott et al., 2008; Scott and Lyons, 2012). Because Mo is a redox-sensitive element, its concentration and isotopic composition has been widely used to infer both local and global redox conditions in ancient oceans (see review by Kendall et al., 2017).

The primary source of Mo to the ocean is oxidative weathering of the upper continental crust, especially ORM and crustal sulfide minerals (molybdenite and especially pyrite because of its greater abundance in the crust; Miller et al., 2011), which leads to the transport of molybdate (MoO_4^{2-}) by rivers ($\delta^{98}Mo$ = 0.2 - 2.3‰, average = 0.7‰; Archer and Vance, 2008) to the oceans (Miller et al., 2011; Scott and Lyons, 2012) (all $\delta^{98}Mo$ values in this section are relative to international standard NIST SRM 3134 = 0.25‰; see section 4.3). Direct groundwater discharge and low-temperature hydrothermal fluids are thought to supply a subordinate flux of Mo to seawater, but their global average Mo concentrations and isotopic compositions are poorly

constrained due to a paucity of data (McManus et al., 2002; Wheat et al., 2002; Miller et al., 2011; King et al., 2016; Neely et al., 2018). Because of the long oceanic residence time of Mo, modern oxygenated seawater has a predominantly uniform Mo isotope composition of 2.34 ± 0.10‰ (Barling et al., 2001; Siebert et al., 2003; Greber et al., 2012; Nakagawa et al., 2012; Goldberg et al., 2013; Nägler et al., 2014).

3.1. Molybdenum concentrations in organic-rich mudrocks

The rate of Mo burial into sediments on the seafloor depends upon the redox state of the bottom waters and sediments. In oxygenated environments, dissolved MoO_4^{2-} is adsorbed onto Fe-Mn oxyhydroxides (as nodules or crusts) accumulating on the deep seafloor with relatively slow sedimentation rates (Barling et al., 2001; Siebert et al., 2003; Barling and Anbar, 2004; Scott and Lyons, 2012). Molybdenum is preferentially buried in suboxic environments ($0.2 < [O_2] < 2$ ml O_2/l H_2O) compared with oxic environments (Scott and Lyons, 2012). Mo forms particle-reactive thiomolybdate complexes in reducing environments where dissolved sulfide is present (Erickson and Helz, 2000). This causes authigenic Mo enrichments in reducing sediments. In the presence of high amounts of sulfide ($[H_2S]_{aq} > 11$ μmol) in euxinic (anoxic and rich in H_2S) bottom waters, Mo converts from molybdate to intermediate thiomolybdate complexes and ultimately to tetrathiomolybdate (Erickson and Helz, 2000). Tetrathiomolybdates are highly particle-reactive and may be rapidly removed to organic matter and sulfide minerals (Helz et al., 1996; Erickson and Helz, 2000; Bostick et al., 2003; Helz et al., 2004; Dahl et al., 2010; Scott and Lyons, 2012). Thiomolybdates may then be converted to reactive Mo-polysulfide species, $Mo(IV)O(S_4)S^{2-}$ or $Mo(IV)S(S_4)S^{2-}$, and this step may include the reduction

of Mo(VI) to Mo(IV) (Dahl et al., 2013). Recent studies suggest that Mo in euxinic environments is buried in the presence of organic matter rather than being incorporated solely into sulfide minerals like pyrite (Chappaz et al., 2014; Dahl et al., 2017; Wagner et al., 2017). The burial rate of Mo in euxinic environments is much more efficient (by 2-3 orders of magnitude) than in oxygenated conditions (Scott et al., 2008; Scott and Lyons 2012; Reinhard et al., 2013). However, the magnitude of Mo enrichment in euxinic sediments also depends on the global seawater Mo concentration and on the rate of Mo recharge to the deep waters in a marine basin, which is influenced by the degree of physical basin restriction from the open ocean (Algeo and Lyons, 2006; Scott and Lyons, 2012).

Molybdenum concentrations in organic-rich sediments are relatively lower in non-euxinic settings than in euxinic settings, which is thus an indicator of local bottom water redox conditions (Scott and Lyons, 2012). Scott and Lyons (2012) concluded the following generalizations to interpret Mo concentrations in ancient black shales and mudrocks: a) Mo enrichments between 1-2 ppm (the upper crustal average) and ~25 ppm indicate that dissolved sulfide was restricted to sediment pore waters, thus indicating non-euxinic bottom waters; b) Mo enrichments above ~25 ppm and below ~100 ppm may reflect a euxinic water column affected by any of four different factors: low concentrations of dissolved Mo in the water column (strong basin restriction or smaller global seawater Mo concentrations in less oxygenated oceans relative to today) (Algeo and Lyons, 2006; Scott et al., 2008), high sedimentation rates (Sageman et al., 2003), seasonally euxinic settings (Francois, 1988), and variations in the pH of the water column (Helz et al., 2011); c) Mo concentrations exceeding ~100 ppm indicates that abundant dissolved Mo and hydrogen sulfide were both present in the water column (Lyons et al., 2003; Scott and Lyons, 2012). A recent study on the Peruvian continental margin shows that Mo concentrations

between 25 ppm and 100 ppm may occur in sediments deposited from anoxic but non-sulfidic bottom waters with dissolved sulfide limited to the sediment pore waters (Scholz et al., 2017).

The ratio of Mo/TOC in euxinic sediments provides information about the paleohydrographic conditions, especially the degree of water mass restriction in anoxic environments (e.g., silled basins) (Algeo and Lyons, 2006). In modern anoxic and euxinic basins, Mo concentrations correlate with the total organic carbon (TOC) concentration in the sediments (Algeo and Lyons, 2006; Lyons et al., 2009). In highly restricted basins, the Mo concentration in bottom waters decreases because the rate of Mo burial into the sediments exceeds the rate of Mo resupply from the open ocean and river inputs (Algeo and Lyons, 2006). In unrestricted marine basins, Mo recharge from the open ocean is rapid, yielding abundant Mo to be removed to sediments, resulting in high Mo concentrations and high Mo/TOC ratios in euxinic sediments. The degree of restriction from weak (Saanich Inlet; 45 ± 5 ppm/wt%) to moderate (Cariaco Basin; 25 ± 5 ppm/wt%) to strong (Black Sea; 4.5 ± 1 ppm/wt%) is thus associated with decreasing Mo/TOC ratios in modern euxinic sediments (Algeo and Lyons, 2006). The slope of the Mo/TOC ratio in euxinic sediments deposited in a local basin partially restricted from the open ocean can be used to interpret temporal and spatial changes in water mass chemistry (Algeo and Lyons, 2006; Reubsam et al., 2017).

The Mo/TOC ratios of black shales and mudrocks deposited in locally unrestricted to weakly restricted euxinic marine settings also provide insight on global ocean redox conditions. High Mo/TOC values in black shales and mudrocks reflect a high-oxygen atmosphere-ocean system, which occurred episodically during the Ediacaran Period and throughout much of the Phanerozoic Eon (Scott et al., 2008; Sahoo et al., 2016). Less oxygenated conditions, including a greater extent of ocean euxinia, prevailed during Phanerozoic ocean anoxic events and

throughout most of the Precambrian. At times of greater ocean anoxia and euxinia compared to today, increased rates of Mo removal to euxinic sediments caused drawdown of the global seawater Mo reservoir, ultimately causing lower Mo/TOC ratios to be recorded in black shales and mudrocks (Scott et al., 2008; Reinhard et al., 2013).

The authigenic Mo-U enrichment patterns could be used to infer different types of marine systems with low oxygen content (Algeo and Tribovillard, 2009). In open ocean conditions, a shift from suboxic to sulfidic benthic conditions results in a stronger enrichment of Mo in sediments than U (***Figure 3***; Algeo and Tribovillard, 2009). This change to more reducing conditions results in the Mo/U ratio in sediments changing from 0.1 - 0.3 times the modern seawater molar ratio to 1 - 3 times the modern seawater molar ratio. In a weakly euxinic basin where an Fe-Mn particulate shuttle is operating, Mo is more strongly adsorbed onto Fe-Mn oxides compared to U. After the Fe-Mn particles reach the sediment, they may be dissolved because of anoxic conditions in the sediment, thus releasing their Mo (and smaller amounts of U), which then be captured by organic matter and authigenic phases (e.g., pyrite) in the sediment. (***Figure 3;*** Algeo and Tribovillard, 2009). However, in strongly restricted basins, instead of a particulate shuttle, the evolution of watermass chemistry plays an important role on controlling Mo-U enrichments in the sediments (Algeo and Tribovillard, 2009). In a basin that has become strongly restricted and developed euxinic bottom waters, Mo is more efficiently removed to the euxinic sediments compared with U, leading to greater drawdown of water column Mo concentrations compared to U. Once steady-state conditions are established in a strongly euxinic basin, the sediment Mo/U ratio in that basin will be lower compared to euxinic sediments in less restricted euxinic basins (***Figure 3;*** Algeo and Tribovillard, 2009).

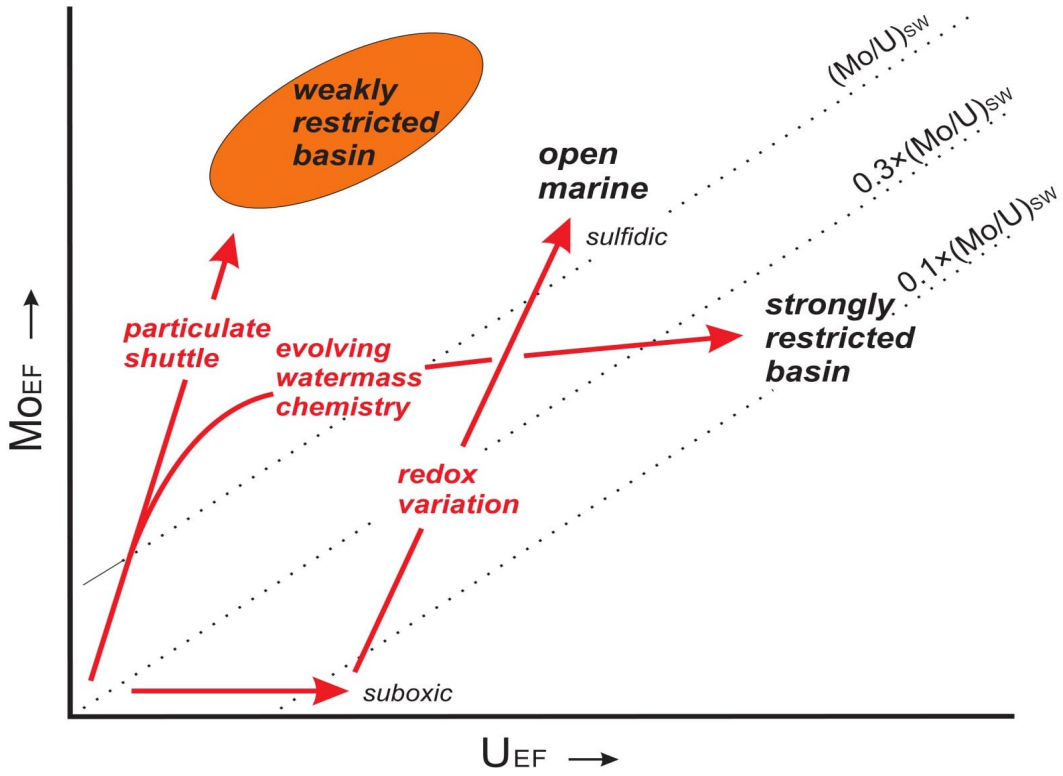

Figure 3. Models of Mo-U enrichment patterns. The dashed lines represent the Mo/U ratios in seawater (modified from Algeo and Tribovillard, 2009).

3.2. Molybdenum isotopes in organic-rich mudrocks

In this section, the distribution of Mo isotopes in marine environments (***Figure 3***) is reviewed because of its importance for understanding the isotopic composition of ORMs. There are three major oceanic sinks for Mo: 1) oxygenated settings where dissolved O_2 penetrates well below the sediment-water interface and Fe-Mn oxides are permanently buried; 2) mildly oxygenated to anoxic settings where bottom waters are oxygenated but dissolved O_2 penetrates < 1 cm below the sediment-water interface and low dissolved H_2S occurs in shallow sediment pore

waters; and 3) euxinic settings where free H_2S is present in the water column and sediments (Scott and Lyons, 2012). The magnitude of Mo isotope fractionation during Mo removal to sediments is different for each of these redox categories (***Figure 4***).

The magnitude of Mo isotope fractionation between seawater ($\delta^{98}Mo$ = 2.3‰) and Mn oxides and crusts ($\delta^{98}Mo$ = –0.7‰) on the seafloor is consistently large, about 3‰, in well-oxygenated settings (Barling et al., 2001; Siebert et al., 2003; Poulson et al., 2006; Siebert et al., 2006). In mild-O_2 to anoxic (non-sulfidic) environments, a wide range of Mo isotope fractionation, 0.3-3‰, occurs between seawater and sediments. A smaller magnitude of isotope fractionation (≤1‰) occurs between seawater and sediments for the case where bottom waters are weakly oxygenated to anoxic/non-sulfidic, and there is high dissolved porewater H_2S, with an average $\delta^{98}Mo$ of ~1.6‰ for the sediments in this environment. In weakly euxinic systems (bottom water $[H_2S]_{aq}$ < 11 μM), light Mo isotopes are preferentially removed into sediments because Mo removal from bottom waters is not quantitative, and the fractionation factor between seawater and the sediment ranges widely from 0.5‰ (deep Cariaco Basin) to 3‰ (shallow Black Sea just below the chemocline) (Arnold et al., 2004; Neubert et al., 2008). The reason for the large $\delta^{98}Mo$ differences between these two weakly euxinic settings is still unsolved. Quantitative removal of Mo from bottom waters with $[H_2S]_{aq}$ > 11 μM may occur (particularly in severely restricted basins with slow rates of deep-water renewal), thus allowing the preservation of global seawater $\delta^{98}Mo$ signatures in euxinic sediments, as observed in the modern Black Sea and the Kyllaren Fjord (Barling et al., 2001; Arnold et al., 2004; Neubert et al., 2008; Noordmann et al., 2015).

In carbonate rocks, Mo concentrations are low (0.004-0.120 ppm) and thus these sedimentary rocks are not a major Mo sink. The $\delta^{98}Mo$ values of carbonates are 0.07-2.19‰

(Voegelin et al., 2009). Corals, a skeletal organism, have a narrow range of Mo concentrations (0.02-0.03 ppm) and δ^{98}Mo values (2.0-2.2‰) that are slightly lower than modern seawater (Voegelin et al., 2009). The Mo isotope composition is ~1‰ lower than seawater and the Mo concentrations are low (< 0.2 ppm) for bulk carbonate sediments (non-skeletal) in shallow water settings with low sulfide concentrations (Romaniello et al., 2016). However, non-skeletal carbonates with high sulfide concentrations have higher Mo concentrations (2-28 ppm) and higher Mo isotope compositions (Romaniello et al., 2016).

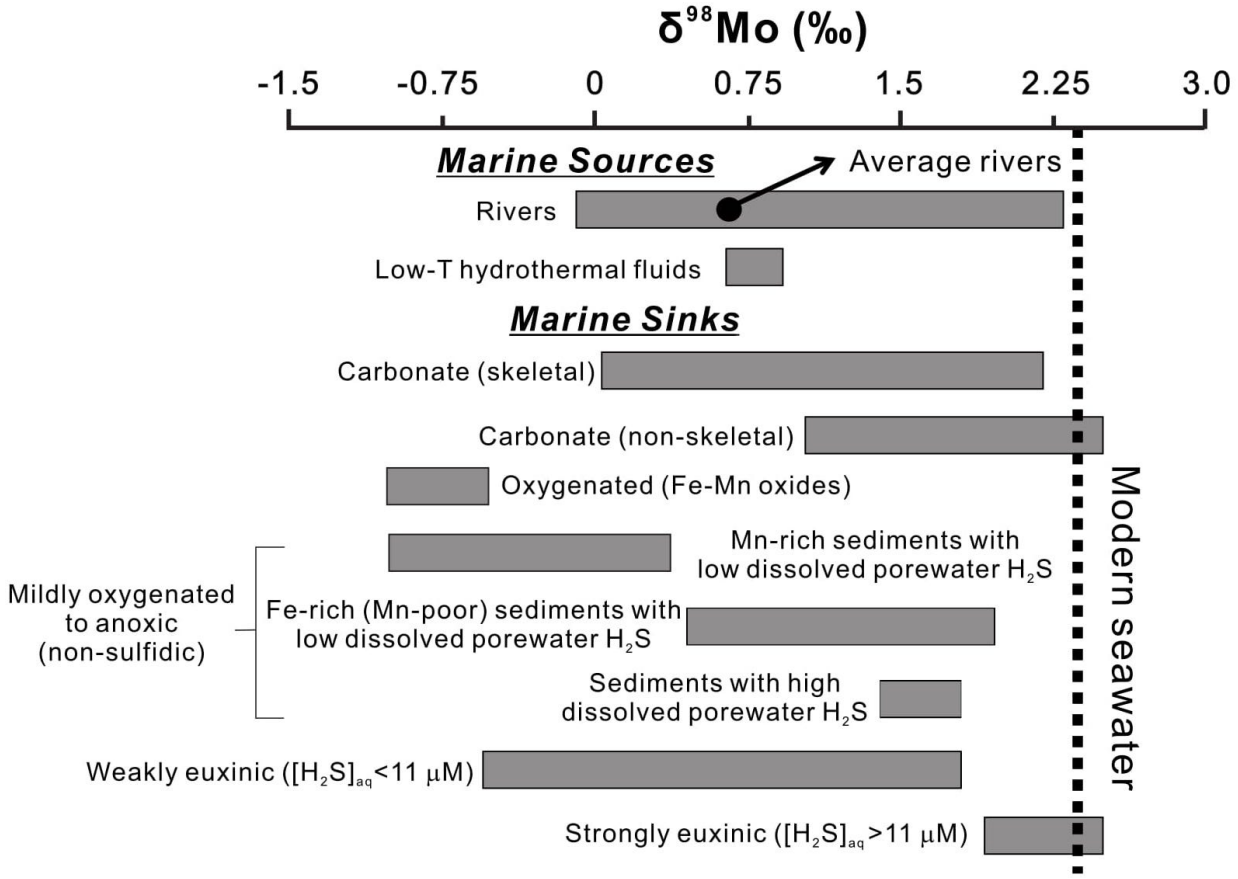

Figure 4. Molybdenum isotope compositions of oceanic inputs and of sediments deposited under different redox conditions in the modern ocean (modified from Kendall et al., 2017).

In the modern ocean (which is predominantly well-oxygenated), it is the oxygenated Mn

oxide sink with its large isotope fractionation of 3‰ that plays a major role in driving modern seawater δ^{98}Mo to higher values than the average river input composition of 0.7‰ (Barling et al., 2001; Arnold et al., 2004; Archer and Vance, 2008). From oxygenated environments to strongly euxinic settings, the Mo isotope compositions become closer to the modern seawater δ^{98}Mo (with the exception of some weakly euxinic sediments) (***Figure 4***; Neubert et al., 2008). Hence, strongly euxinic sediments and their lithified equivalents (ORM) have the best chance of directly capturing the Mo isotope signature of coeval seawater if the removal of Mo from local bottom seawater is quantitative (Kendall et al., 2017). However, it is hard to interpret the concentration of H_2S in ancient bottom waters or to determine if the Mo removal from bottom waters was quantitative (Barling et al., 2001; Arnold et al., 2004; Nägler et al., 2011; Noordmann et al., 2015). Euxinic ORM with lower Mo concentrations deposited in more restricted basins are more likely to reflect conditions of quantitative Mo removal from bottom waters and thus capture the seawater δ^{98}Mo signature. However, for euxinic ORM with higher Mo concentrations, the δ^{98}Mo has to be a minimum for seawater δ^{98}Mo because any non-quantitative Mo removal from the water column causes a Mo isotope fractionation, with lighter Mo isotopes preferentially removed to sediments (Arnold et al., 2004). For strongly euxinic conditions ($[H_2S]_{aq} > 11\mu M$) where Mo removal is not quantitative, the fractionation factor may be about 0.5 ± 0.3‰ (Nägler et al., 2011). For weakly euxinic conditions ($[H_2S]_{aq} < 11\mu M$), the fractionation factor can be larger because of the combined effects of non-quantitative Mo removal and incomplete conversion from molybdate to tetrathiomolybdate (Arnold et al., 2004; Neubert et al., 2008). Hence, if the Mo removal was not quantitative and/or weakly euxinic conditions prevailed, then the δ^{98}Mo of euxinic black shales and mudrocks could be lower than coeval global seawater δ^{98}Mo. In this scenario, the coeval seawater δ^{98}Mo is most closely approximated by the highest δ^{98}Mo value

found in an ancient ORM stratigraphic interval (Dahl et al., 2010; Kendall et al., 2015).

Taking these caveats into consideration, low Mo concentrations and low δ^{98}Mo in euxinic black shales and mudrocks can point to more widespread ocean anoxia than today. By contrast, high Mo concentrations and high δ^{98}Mo are considered an indicator for a well-oxygenated global ocean with anoxic settings confined to restricted basins and oxygen minimum zones in highly productive ocean margins (Lyons et al., 2003; Arnold et al., 2004; Algeo and Lyons, 2006; Scott et al., 2008; Nägler et al., 2011; Scott and Lyons, 2012).

3.3. Molybdenum oil geochemistry

Crude oils can be sub-divided into multiple organic components, including saturates, aromatics, resins, and asphaltenes according to their polarizability and polarity (Tissot and Welt, 1978). The maltene fraction includes aromatics, saturates, resins, and is soluble in *n*-heptane and *n*-pentane, whereas the asphaltene fraction is insoluble in *n*-heptane and *n*-pentane (Tissot and Welt, 1978; Speight et al., 1994; Speight and Long, 1995). Asphaltene has the highest molecular weight and is the most complex fraction in crude oils, as it contains aromatic rings, heterogeneous molecules, and heteroatomic species that contain oxygen, nitrogen, or sulfur (Rogel, 2000; Yarranton et al, 2000; Murgich et al, 1999; Calemma et al, 1995). Trace metal constituents in petroleum exist in oils as oil-soluble organometallic substances (Karchmer and Gunn, 1952). Previous studies show that metals are generally concentrated in the asphaltene fraction of oil but can also be found in the maltene fraction (e.g., resins and aromatics; Filby and Van Berkel, 1987; Filby, 1994; Duyck et al., 2002; Selby et al., 2007; DiMarzio et al., 2018). The complexation of metals in asphaltene are poorly understood, but may be primarily bound to

heteroatomic species that contain oxygen, nitrogen, or sulfur (Baker, 1969; Yen, 1975). Vanadium and nickel, the two most abundant elements in oil, are also known to exist as metalloporphyrins, which can occur in both the asphaltene and maltene fractions (Nordgard et al, 2009; Trejo and Ancheyta, 2007).

Previous studies suggest that the Mo is fixed to O- and S-containing organic molecules in oils, kerogens, and bitumens, although the exact chemical speciation of Mo in crude oil is poorly understood and is largely inferred based on understanding of Mo complexation to sulfurized organic matter in organic-rich mudrocks (Filby, 1994; Ventura et al., 2015; Dimarzio et al., 2018). Crude oils sourced from Phanerozoic aged sedimentary basins in Russia, Kuwait, USA, Venezuela, and Brazil have Mo concentrations of 0.011-1.44 ppm (Ventura et al., 2015). In a recent study, a heavy crude oil from the Gela field (Sicily, Italy) was separated into *n*-heptane insoluble (asphaltene) and soluble (maltene) fractions (DiMarzio et al., 2018), primarily to study the distribution of Re and Os in different oil fractions, but other metals were also examined, including Mo. The authors also measured metal contents in the resins absorbed on the *n*-heptane-insoluble fraction. The Mo concentrations in the asphaltene, maltene, and absorbed resins in the oil are 136 ppm, 0.808 ppm, and 1.563 ppm, respectively (DiMarzio et al., 2018). Hence, Mo is concentrated in the asphaltene fraction. DiMarzio et al. (2018) concluded that about 98% of Re and Os are concentrated in asphaltene, which is consistent with previous Re-Os studies (Selby et al., 2007; Georgiev et al., 2016; DiMarzio et al., 2018). The electronegativities of Mo (2.16), Cd (1.69), Re (1.9), and Os (2.2) are similar, and the ionic radii of reduced forms of Mo, Cd, Re, and Os are also close (DiMarzio et al., 2018). This might explain why the behavior and distribution of Mo and Cd are close to Re and Os in asphaltene and its sub-fractions (DiMarzio et al., 2018).

Like Re and Os, Mo is concentrated most strongly in the most polar-aromatic sub-fractions of asphaltene (DiMarzio et al., 2018).

Limited Mo isotope data exists for crude oils. In an abstract, it was reported that the δ^{98}Mo of co-genetic oil samples (from an un-named petroleum system) for different alteration gradients (with only maturity given as an example) have almost the same value, and thus the Mo isotope composition of oils has potential application as a tracer for oil-oil and source rock-oil correlations (Archer et al., 2012). In the only published paper on Mo isotopes, oils produced from the lacustrine source rocks of the Campos Basin in Brazil have δ^{98}Mo values of -0.21‰ to 0.88‰. The precision of these δ^{98}Mo values (2SD), based on full procedural replicate analyses, ranged from ± 0.12‰ to 0.56‰ (Ventura et al., 2015), which is higher than the typical precision of δ^{98}Mo measurements on source rocks (typically <0.12‰; Kendall et al., 2017). The δ^{98}Mo values in oils from the Campos Basin were compared with δ^{98}Mo values in known Earth reservoirs (lacustrine sediments, marine sediments, major rivers, seawater, granites and basalts) by Ventura et al. (2015), but no Mo isotope data was presented for the actual lacustrine source rocks in the Campos Basin. Mo isotopes might not be a good oil-source rock tracer because the Campos Basin oils have a wide range of Mo isotope values that extend to lower values than those normally found in black shales (Ventura et al., 2015). Hence, Mo isotopes may have a greater role as a tracer of migration or reservoir processes (Ventura et al., 2015).

However, Archer et al. (2012) found that δ^{98}Mo was invariant in co-genetic oil samples for various alteration gradients and suggested that Mo has potential application as a tracer for oil-source rock correlation (Archer et al., 2012). The Mo isotope compositions of different source rocks are controlled by local and global redox conditions during sediment deposition, as described in section 3.2. Oils may then be correlated to a source rock with a similar Mo isotope

composition. However, oils may be derived from multiple source rocks. A simple mass balance equation can help to determine the relative proportion of oil supplied by different source rocks only if the source rocks have a narrow range of discrete Mo isotope values. However, if source rocks have a wide range of overlapping Mo isotope compositions, then the mass balance equation cannot be used in this situation.

4. Methods

4.1. Samples

4.1.1. Meade Peak Member and Retort Member Source Rocks

Fourteen samples of black shale or massive organic-rich mudstone were collected from the two major oil source rocks in the Phosphoria Formation: nine samples from the Meade Peak Member and five samples from the Retort Member (**Table 4**). Organic-rich mudstones from the Meade Peak Member are grey or black, and the dolomitic/calcareous samples are light-medium grey in color. Mudstones from the Retort Member are all massive and are not dolomitic or calcareous. For each Member, samples were collected from two or three outcrop locations to obtain a regional perspective on geochemical variations (**Table 4; Figure 1**). The source rock samples are thermally immature to overmature with respect to temperatures for hydrocarbon generation (P. Lillis, pers. comm., 2016). Specifically, the Astoria, Crystal Creek, Beaverhead, and Slide Lake localities are thermally overmature, mature, mature, and immature, respectively (see **Table 4** for a list of samples at each locality). Material selected for analysis from the black shale and mudstone samples did not include diagenetic/hydrothermal macroscopic quartz/carbonate veins, macroscopic pyrite nodules, and weathered material because these features would affect the use of geochemical results to reconstruct the depositional environment. Organic-rich shales and mudstones ranging in age from Archean to Phanerozoic that are free of these diagenetic/hydrothermal/weathered features and have experienced no more than lower greenschist facies metamorphism have routinely yielded precise and accurate Re-Os depositional ages (Kendall et al., 2009b). Given the similarities in geochemical behavior (redox-sensitive, association with sulfides and organic matter in shales and mudstones) between Mo and Re-Os, the Mo concentration and isotope composition of such well-preserved shales and mudstones

should reflect depositional conditions. To evaluate the degree of Mo concentration and isotope heterogeneity at the hand sample scale, two of the Meade Peak samples were each cut into three pieces (15PGL0831-001(A), 15PGL0831-001(B), 15PGL0831-001(C); 15PGL0831-002(A), 15PGL0831-002(B), 15PGL0831-002(C)). Similarly, three Retort Member samples were each cut into two pieces (15PGL0901-002(A), 15PGL0901-002(B); 15PGL0901-003(A), 15PGL0901-003(B); 15PGL0901-007(A), 15PGL0901-007(B)). The samples were analyzed for total organic carbon content, major/minor/trace element abundances, and Mo isotope compositions.

Table 4. Lithological descriptions and locations of mudstone samples from the Phosphoria Formation

	Sample	Lithology	Location Description	County State	Latitude (N)	Longitude (W)
Meade Peak Member	15PGL0831-001	mudstone, dark,	Astoria roadcut	Teton, Wyoming	43.30	-110.78
	15PGL0831-002	mudstone, dark, massive	Astoria roadcut	Teton, Wyoming	43.30	-110.78
	16PGL0914-01	mudstone, medium gray, massive, non-calcareous	Crystal Creek	Teton, Wyoming	43.56	-110.40
	16PGL0914-02	mudstone, med.-dark gray, massive, dolomitic	Crystal Creek	Teton, Wyoming	43.56	-110.40
	16PGL0914-03	mudstone, dark gray, massive, non-calcareous	Crystal Creek	Teton, Wyoming	43.56	-110.40
	16PGL0914-04	mudstone, dark gray, platy, dolomitic	Crystal Creek	Teton, Wyoming	43.56	-110.40
	16PGL0914-05	mudstone, medium gray, weakly bedded	Crystal Creek	Teton, Wyoming	43.56	-110.40
	16PGL0914-06	mudstone, med.-dark gray, blocky, dolomitic	Crystal Creek	Teton, Wyoming	43.56	-110.40
	16PGL0914-07	mudstone, light-med gray, dolomitic to calcareous, calcite veins	Crystal Creek	Teton, Wyoming	43.56	-110.40
Retort Member	070621-2	mudstone, dark gray, massive		Beaverhead, Montana	45.03	-112.68
	15PGL0901-002	mudstone, dark, massive	Crystal Creek	Teton, Wyoming	43.56	-110.40
	15PGL0901-003	mudstone, dark, massive	Crystal Creek	Teton, Wyoming	43.56	-110.40
	15PGL0901-004	mudstone, dark, massive	Crystal Creek	Teton, Wyoming	43.56	-110.40
	15PGL0901-007	mudstone, dark, massive	Slide Lake	Teton, Wyoming	43.64	-110.57

4.1.2. Oils and Asphaltenes

Oil and asphaltene samples analyzed in this study are the same as the samples studied for Re-Os isotopes by Lillis and Selby (2013). The samples were described in section 2.2 and are shown in **Table 1**. Nineteen Phosphoria-sourced oil samples were collected from the Bighorn Basin (locations are shown in ***Figure 2***). The oils are from the Cloverly Formation, Tensleep Formation, Bighorn Dolomite Formation, Madison Formation, Amsden Formation, and Phosphoria Formation (**Table 1**). For eight of the nineteen oils, the asphaltene fraction was separated as described in Lillis and Selby (2013) (see section 4.2.2).

4.2. Elemental analyses

4.2.1. Source Rocks

The source rock, oil and asphaltene separates were dissolved and their metal concentrations were measured at the Metal Isotope Geochemistry Laboratory, Department of Earth and Environmental Sciences, University of Waterloo. First, the source rock samples were broken into small chips without metal contact and were powdered using metal-free methods in an automated agate ball mill. A known amount (100-125 mg) of black shale or mudrock sample powder was ashed for 24 hours at 550°C to remove organic matter via oxidation to CO_2. Subsequently, the ashed sample powder was transferred from crucibles to 22 mL Savillex Teflon beakers and digested in concentrated HCl-HNO_3-HF in a metal-free clean lab. Samples were digested first in 2.5 mL HNO_3 and 0.5 mL HF for 48 hours at 110°C, followed by 1 mL HNO_3 and 3 mL HCl for 48 hours at 110°C. Finally, 2 mL of HCl were added to the samples for 24 hours at 110°C. After dry-down, the sample solutions were stored in 5 mL 6M HCl and 3 drops of 0.5% HF.

An aliquot of the digested sample solution was then diluted in 2% HNO_3 for analysis of the element concentrations on an Agilent 8800 triple quadrupole inductively coupled plasma mass spectrometer (QQQ-ICP-MS). Instrument drift during each measurement session was corrected using Sc, Ge, In, and Bi as internal standards. Instrument accuracy was verified by analysis of three black shale standards processed in the same manner as samples: United States Geological Survey (USGS) SBC-1 (Pennsylvanian Brush Creek Shale), SGR-1b (Eocene Green River Shale), and SDO-1 (Devonian Ohio Shale). The measured elemental concentrations of samples were corrected based on the average recovery rate obtained from comparison of certified standard values with the measured elemental concentrations of the three black shale standards. Full powder replicate analyses were also done for a few organic-rich mudrock samples. For each individual sample analysis, the % relative standard deviation (%RSD) was <4%. For the multiple analyses of each black shale standard (SBC-1, SGR-1b, and SDO-1), the %RSD on the mean elemental concentration was <4%. A total procedural blank for rock digestion had a Mo content of 0.844 ng that is < 1% of the measured sample Mo contents. Likewise, low blank levels (< 1%, many < 0.01%) were also observed for other elements analyzed in this study.

To help evaluate local redox conditions, element enrichment factors (EF) were calculated relative to average upper crust to correct the influence of variable carbonate and detrital content in the samples. The EF was calculated using the following equation (average upper crust abundance (AUCA): Al = 80,400 ppm, Mo = 1.5 ppm, U = 2.8 ppm; McLennan, 2001; Tribovillard et al., 2006):

$$EF = [metal / Al]_{sample} / [metal / Al]_{average\ upper\ crust}$$

Total organic carbon (TOC) contents of the source rock samples were measured at the Agricultural and Food Laboratory, University of Guelph. To measure total inorganic carbon

content, samples were first ashed at 475°C for 3 hr to remove organic matter, and then analyzed using catalytic combustion at 960°C on an Elementar Vario Macro Cube CN combustion analyzer. Inorganic carbon components were separated from other gases and analyzed using thermal conductivity detection. Total carbon contents were measured on a separate split of sample powder at 960°C without the use of an ashing step. Total organic carbon contents were calculated as the difference between total carbon and total inorganic carbon. Instrument accuracy was assessed by two analyses of the USGS standard SBC-1, which yielded TOC values of 1.36-1.37 wt% (the certified value is 1.23 ± 0.02 wt%; 1SD).

4.2.2. Oils and asphaltenes

Asphaltenes were precipitated from bulk oils by mixing with iso-octane at a ratio of 40 parts per 1 part crude oil (Lillis and Selby, 2013). After mixing continuously overnight (Selby et al., 2007), the insoluble asphaltene precipitates were separated from the residual oil by centrifugation and then filtered using 0.45-micron PTFE syringe filters that were attached to a Luer-Loc glass syringe. Subsequently, the asphaltenes were dissolved using $CHCl_3$, filtered, dried, and weighed (Lillis and Selby, 2013).

Oil digestion aims to reduce the heterogeneity and viscosity of oil samples, which is challenging because of the complex organic compositions. The asphaltene separates and bulk crude oils were dissolved in concentrated HNO_3 at high temperature and pressure in an ULTRAWAVE microwave digestion system. Prior to extracting the oil for digestion, the sample vials were warmed by hand to reduce the viscosity of the oil. Subsequently, 0.045 g to 0.338 g of each crude oil sample and 0.00773 g to 0.317 g of each asphaltene separate was put into

microwave quartz tubes, together with 5 ml concentrated HNO_3 and 1 mL Milli-Q water. Two back-to-back rounds of microwave digestion (i.e., without adding additional acid to the samples between digestions) were carried out to maximize dissolution of the oils and asphaltenes. The oil sample solutions were a light green color after the two rounds of microwave digestion. After microwave digestion, sample solutions were dried and then ashed in a muffle furnace at 550°C overnight to remove any remaining organic matter from the samples, which helps reduce matrix effects during mass spectrometry analysis. Subsequently, oil and asphaltene samples were re-digested in 1 mL HNO_3 and 3 mL HCl for 48 hours at 110°C. After drying, the sample solutions were stored in 5 mL 6M HCl and 3 drops of 0.5% HF.

All oil and asphaltene samples were measured for elemental concentrations using QQQ-ICP-MS. National Institute of Standards and Technology (NIST) Reference Material (RM) 8505 (heavy oil) was analyzed along with samples. The certified V concentration of NIST RM 8505 is 390 ± 10 ppm. The measured average V concentration in this study is 378.12 ppm (SD = 8.38 ppm, n=2), which indicates the accuracy of our analytical procedure. For oil and asphaltene sample analysis, most of the %RSD was <6%, and usually <1%. The %RSD for all analyses of oil standard RM 8505 was mainly < 6%. Total procedural blanks of oil measurements contained an average Mo content of 2.73 ng (SD = 0.910 ng). Blanks are < 10% of the measured Mo contents in many sample oils. For measured Mo concentrations of below 42 ppb in the rest of the oil samples, however, the blanks constituted >32% of the measured total Mo content. Total procedural blanks of asphaltene measurements contained an average Mo content of 6.45 ng. Blanks are < 10% of the measured total Mo contents in sample asphaltenes except for some asphaltenes with extremely low Mo concentrations. For measured total Mo concentrations of below 1000 ppb in the rest of the asphaltene samples, the blank was >12% of the measured Mo

content. Blanks are <3% of the measured V contents in both oils and asphaltenes, and <4% of the measured Ni contents in both oils and asphaltenes. The oil and asphaltene samples with total measured Mo contents of < 10 ng were not analyzed for Mo isotopes because these samples with high blank levels are not reliable for isotope analysis.

In addition to QQQ-ICP-MS analyses, Mo concentrations were more precisely calculated using the results of double spike analysis associated with measurement of oil and asphaltene samples for Mo isotope compositions, which is described in the section below.

4.3. Mo isotopes

Molybdenum was isolated from the digested bulk oil, asphaltene, and source rock samples using a two-stage anion exchange and cation exchange chromatography protocol at the Metal Isotope Geochemistry Laboratory, following procedures described in Barling et al. (2001), Arnold et al. (2004), and Duan et al. (2010). A ^{97}Mo-^{100}Mo double spike solution was added to each sample before column chemistry to correct for the mass fractionation that occurs during column chromatography and instrumental analysis. For column chemistry, 0.5 ml of the ~ 1 ppm ^{97}Mo-^{100}Mo double spike solution was added to the 6M HCl sample solutions containing 250 ng Mo for source rock samples or 100 ng Mo for oil and asphaltene samples. BioRad AG1X8 100-200 mesh resin was used for Mo anion column chemistry, and removed most elements from the sample solution. When the acid strength was changed from 6M HCl to 1M HCl, Mo and Fe were released from the resin, whereas other elements remained stuck to the resin. BioRad AGWX8 200-400 mesh resin was used for Mo cation column chemistry. The solution containing Mo and Fe released by anion column chemistry was dried, re-dissolved in 0.5M HCl, and added to the cation exchange resin. Subsequently, the cation resin was washed with 0.5M HCl and 0.01%

H_2O_2, which allows Mo to pass straight through the column while Fe is stuck to the resin. After each column chemistry step, samples were dried and reacted twice with a mixture of HNO_3-H_2O_2 to destroy any organic material incorporated into the sample from the resins.

Molybdenum isotope compositions were measured on a Thermo Neptune multi-collector inductively coupled plasma mass spectrometer (MC-ICP-MS) at the W.M. Keck Foundation Laboratory for Environmental Biogeochemistry, School of Earth and Space Exploration, Arizona State University (ASU). Sample δ^{98}Mo is reported relative to the international NIST SRM 3134 standard (Goldberg et al., 2013; Nägler et al., 2014) as shown by the equation below:

$$\delta^{98}\text{Mo (‰)} = 1000 \times [(^{98/95}\text{Mo})_{\text{sample}} / (^{98/95}\text{Mo})_{\text{NIST SRM 3134}}] - 1] + 0.25$$

The NIST SRM 3134 standard is set to 0.25‰ instead of 0‰ (Nägler et al., 2014). Relative to this standard, global oxygenated seawater today has a δ^{98}Mo of 2.34 ± 0.10 ‰ (Arnold et al., 2004; Goldberg et al., 2013; Nägler et al., 2014). Instrument accuracy and reproducibility were checked through analyses of the Devonian Ohio Shale standard SDO-1 (long-term average δ^{98}Mo = 1.07 ± 0.11 ‰ relative to NIST SRM 3134 = 0.25‰; 2SD; n=145; based on double spike analyses at Arizona State University; Goldberg et al., 2013). In this study, the measured δ^{98}Mo value for SDO-1 is 1.00 ± 0.02 ‰ (n=4) relative to NIST SRM 3134 = 0.25 ‰. The standards SBC-1 (Brush Creek Shale) and SGR-1b (Green River Shale) from the USGS also were analyzed to develop them as secondary standards because SDO-1 is no longer commercially available. The measured δ^{98}Mo values for SBC-1 and SGR-1b are 0.64 ± 0.02‰ (n=3) and 0.58 ± 0.02‰ (n=3), respectively. The 2SD uncertainty of a sample is either the 2SD uncertainty of sample replicate measurements or 0.11‰ (the long-term uncertainty of SDO-1), whichever is greater.

5. Results

5.1. Elemental concentrations and Mo isotope data for the source rocks

The TOC contents, major, minor, and trace elemental concentrations, and Mo isotope compositions for the Phosphoria Formation source rocks are shown in **Table 5** and **Table 6**. The Meade Peak Member has TOC contents between 0.4% and 8.7%, whereas the Retort Member has TOC contents between 2.4% and 16.6%. Regional variations are observed in TOC content for both Members. The highest TOC content of 16.6% in the Retort Member is from a single sample collected from an outcrop in Beaverhead County, Montana. The other Retort Member samples from the Crystal Creek and Slide Lake localities in Teton County, Wyoming, have lower TOC contents of 2.4-4.0% (these two localities have overlapping TOC contents). Meade Peak Member samples from the Astoria roadcut in Teton, Wyoming, have higher TOC contents (5.9–8.7%) than other Meade Peak Member samples from the Crystal Creek locality (0.4–2.2%).

Redox-sensitive elemental concentrations and Mo isotope compositions of the Retort Member exhibit significant differences between the localities. The single Retort Member sample from Beaverhead, Montana, with the higher TOC content also has higher concentrations and EFs of Mo (59.6 ppm; EF = 85.9), U (36.1 ppm; EF = 27.9), V (326.9 ppm; EF = 6.60), and EF of Ni (EF = 5.70). Other Retort Member samples have lower concentrations and EFs of Mo (9.58-41.7 ppm; EF = 12.5-43.5), U (5.12-10.2 ppm; EF = 3.60-7.76), V (53.0-266 ppm; EF = 1.86-4.37), and EF of Ni (EF = 2.72-5.08). There is overlap in the concentrations and EFs of Zn (86.8-952.3 ppm; EF = 4.58-21.2) and concentrations of Ni (52.7-142.4 ppm) between the three sampled localities for the Retort Member. The δ^{98}Mo of the Retort Member samples range from 1.05‰ to 1.98‰. The TOC-rich sample from Beaverhead has an intermediate δ^{98}Mo value (1.48‰)

compared to the lower-TOC Retort Member samples. The lowest δ^{98}Mo values are observed in the sample with the lowest Mo concentrations and EFs (Slide Lake locality).

For the Meade Peak Member, the Astoria samples have higher concentrations and EFs of Mo (52.2-443 ppm; EF = 63.6-607), U (9.0-35.7 ppm; EF = 5.86-22.6), V (485-6756 ppm; EF = 8.29-115), and Zn (770-1130 ppm; EF = 15.8-28.9) compared with the Crystal Creek samples. There is some overlap in Ni concentrations and EFs between the two Meade Peak Member localities, although higher values are observed more commonly for the Astoria locality (106-496 ppm; EF = 4.38-23.17) than the Crystal Creek locality (13.29-237 ppm; EF = 1.07-24.5). Two samples from the Crystal Creek locality (16PGL0914-06 and 16PGL0914-07) have unusually low Al contents (0.3 wt%) as well as usually high Ca (20-21 wt%) and Mg (10-11 wt%) contents, and are thus more carbonate-rich compared with the other Meade Peak Member samples, resulting in spuriously high EFs for Mo, U, V, Zn, and Ni. The δ^{98}Mo values in the Meade Peak Member range between 0.37‰ and 2.27‰. The Mo- and TOC-rich Astoria samples have generally higher δ^{98}Mo values (1.42‰ to 1.77‰) compared to the Mo- and TOC-poor Crystal Creek samples (0.37-0.87‰; except for one sample with a value of 2.27‰).

The TOC-rich samples of the Retort Member and Meade Peak Member are most likely to influence the Mo isotope composition of oils produced from these units. All samples from the Retort Member as well as the Astoria roadcut samples from the Meade Peak Member have TOC contents of at least 2.4 wt%. These TOC-rich samples span an overall range in δ^{98}Mo of 1.05‰ to 1.98‰. No significant difference in the δ^{98}Mo values is observed between the TOC-rich samples of the Retort Member and the Meade Peak Member.

In this study, variation in elemental concentrations and Mo isotope compositions was also examined at the hand sample scale for five samples from the Retort Member and Meade Peak

Member. Elemental concentrations of two or three sub-samples (derived from a single hand sample) showed examples of both small and large variations, but in all cases, the variation in δ^{98}Mo values at the hand sample scale was not resolvable outside of the long-term instrument reproducibility for Mo isotope measurements (0.11‰). The variability in elemental and isotopic data at the hand sample scale is significantly smaller compared to the total dataset.

Table 5. Trace metal concentrations and Mo isotope data for the black shales from the Phosphoria Formation

Formation	Sample	TOC[a] wt%	Mo ppm	U Ppm	V ppm	Zn ppm	Ni ppm	Mo EF[e]	U EF	V EF	Zn EF	Ni EF	$\delta^{98}Mo$[b] ‰	2SD Measured	2SD[c] Reported	n[d]
Meade Peak Member	15PGL0831-001(A)	7.38	443	29.7	5823	998	496	607	21.8	111	28.9	23.2	1.42	0.02	0.11	3
	15PGL0831-001(B)	7.86	251	34.8	6756	800	421	304	22.6	114	20.5	17.4	1.46	0.03	0.11	3
	15PGL0831-001(C)	8.71	258	35.7	6419	769	366	250	18.5	87.2	15.8	12.1	1.50	0.01	0.11	3
	15PGL0831-002(A)	6.05	57.3	9.80	502	892	106	69.5	6.36	8.53	22.9	4.38	1.77	0.03	0.11	3
	15PGL0831-002(B)	5.94	52.2	8.98	485	913	110	63.6	5.86	8.73	24.2	4.58	1.75	0.03	0.11	3
	15PGL0831-002(B)(rpt)		57.7	9.87	561	1031	128	64.1	5.87	8.72	24.2	4.84	1.69	0.02	0.11	3
	15PGL0831-002(C)	5.94	59.7	10.0	534	1130	133	67.9	6.12	8.51	27.1	5.14	1.74	0.01	0.11	3
	16PGL0914-01	2.20	1.08	1.77	39.7	52.3	13.3	4.60	4.03	2.37	4.70	1.93	0.63	0.05	0.11	3
	16PGL0914-02	1.47	1.52	1.64	39.2	101	35.6	7.62	4.59	2.87	11.1	6.34	2.27	0.03	0.11	3
	16PGL0914-03	1.13	2.88	5.10	107	236	111	4.87	4.62	2.55	8.42	6.38	0.51	0.05	0.11	3
	16PGL0914-03(rpt)		3.01	4.96	107	243	111	5.04	4.45	2.52	8.59	6.32	0.51	0.04	0.11	3
	16PGL0914-04	1.63	5.77	8.51	198	438	237	8.26	6.52	3.97	13.2	11.5	0.87	0.04	0.11	3
	16PGL0914-05	1.44	3.61	3.92	110	148	26.3	4.32	2.52	1.86	3.75	1.07	0.78	0.01	0.11	3
	16PGL0914-06	0.875	5.44	1.84	110	99.5	36.8	106	19.2	30.2	41.0	24.5	0.37	0.05	0.11	3
	16PGL0914-07	0.365	8.08	2.75	180	257	33.5	137	25.0	42.9	92.4	19.4	0.50	0.02	0.11	3
Retort Member	070621-2	16.6	59.6	36.1	327	359	116	85.9	27.9	6.60	10.9	5.70	1.48	0.01	0.11	3
	15PGL0901-002(A)	3.39	24.0	9.56	203	476	98.3	36.4	7.76	4.31	15.2	5.08	1.38	0.01	0.11	3
	15PGL0901-002(A)(rpt)		24.0	9.45	209	470	98.9	35.8	7.55	4.37	14.8	5.03				
	15PGL0901-002(B)	2.99	30.0	10.2	183	748	92.6	40.1	7.29	3.45	21.2	4.23	1.32	0.02	0.11	3
	15PGL0901-003(A)	4.04	39.0	7.48	255	812	142	35.0	3.60	3.22	15.4	4.35	1.62	0.01	0.11	3
	15PGL0901-003(B)	3.96	41.7	8.23	266	952	141	37.4	3.95	3.35	18.0	4.29	1.61	0.02	0.11	3
	15PGL0901-004	2.39	17.4	5.12	53.0	86.8	52.7	43.5	6.85	1.86	4.58	4.48	1.98	0.01	0.11	3
	15PGL0901-007(A)	2.39	9.58	8.16	148	594	71.6	12.5	5.72	2.72	16.4	3.19	1.06	0.06	0.11	3
	15PGL0901-007(B)	3.2	11.0	6.76	132	385	53.1	16.5	5.44	2.79	12.2	2.72	1.05	0.04	0.11	3
Standards	SDO-1		154	47.2	164	51.9	95.1	131	21.5	1.95	0.933	2.76	1.04	0.02	0.11	4
	SDO-1		148	46.9	160	63.1	94.1	123	20.8	1.86	1.11	2.66				
	SBC-1		2.05	5.81	220	125	82.7	0.910	1.38	1.37	1.18	1.25	0.64	0.02	0.11	3
	SBC-1		2.17	5.84	215	183	81.2	1.06	1.52	1.47	1.88	1.35				
	SGR-1b		35.0	5.52	127	112	30.3	57.6	4.87	2.92	3.90	1.70	0.58	0.02	0.11	3
	SGR-1b		34.6	5.53	133	76.5	31.1	53.1	4.54	2.86	2.48	1.62				

[a] TOC = Total Organic Carbon
[b] Mo isotope data reported relative to international standard NIST SRM 3134 = 0.25‰
[c] Reported uncertainty is the 2SD of replicate measurements or 0.11‰, whichever is greater
[d] Number of times the sample solution was analyzed (in different analytical sessions)
[e] Enrichment Factor

Table 6. Major/minor element concentrations for the black shales from the Phosphoria Formation

Formation	Sample	Na wt%	Mg wt%	Al wt%	P wt%	K wt%	Ca wt%	Ti wt%	Mn wt%	Fe wt%
Meade Peak Member	15PGL0831-001(A)	0.071	0.410	3.91	0.204	1.70	2.72	0.343	0.003	2.04
	15PGL0831-001(B)	0.074	0.470	4.54	0.198	1.94	2.99	0.396	0.003	0.811
	15PGL0831-001(C)	0.080	0.520	5.53	0.222	2.23	3.50	0.421	0.004	1.06
	15PGL0831-002(A)	0.074	2.64	4.42	0.058	2.24	3.99	0.342	0.021	1.96
	15PGL0831-002(B)	0.070	2.63	4.40	0.058	2.10	4.05	0.332	0.020	1.89
	15PGL0831-002(B)(rpt)	0.086	3.06	4.83	0.063	2.58	4.24	0.375	0.023	2.21
	15PGL0831-002(C)	0.085	2.83	4.71	0.067	2.44	4.05	0.346	0.021	2.09
	16PGL0914-01	0.081	6.47	1.26	0.170	0.859	11.8	0.089	0.016	0.584
	16PGL0914-02	0.095	5.42	1.03	0.125	0.593	10.1	0.069	0.007	0.456
	16PGL0914-03	0.099	5.75	2.19	0.230	1.45	10.5	0.195	0.009	1.00
	16PGL0914-03(rpt)	0.120	5.05	3.15	0.289	2.11	9.35	0.202	0.010	1.76
	16PGL0914-04	0.146	5.28	3.75	0.336	2.53	10.2	0.204	0.009	1.01
	16PGL0914-05	0.072	0.53	4.47	0.095	3.29	0.817	0.350	0.003	0.844
	16PGL0914-06	0.105	10.8	0.275	0.027	0.275	20.7	0.026	0.010	0.295
	16PGL0914-07	0.082	10.2	0.315	0.052	0.425	19.7	0.036	0.014	0.503
Retort Member	070621-2	0.076	0.323	3.72	2.30	1.24	3.59	0.275	0.004	1.62
	15PGL0901-002(A)	0.113	1.57	3.54	0.626	2.19	3.04	0.215	0.014	1.78
	15PGL0901-002(A)(rpt)	0.140	1.63	3.60	0.646	2.26	3.07	0.218	0.015	1.83
	15PGL0901-002(B)	0.130	1.91	4.00	0.780	2.55	3.68	0.233	0.017	2.04
	15PGL0901-003(A)	0.158	2.15	5.98	0.691	3.41	3.84	0.341	0.024	2.86
	15PGL0901-003(B)	0.169	2.23	6.07	0.826	3.49	4.24	0.357	0.025	2.88
	15PGL0901-004	0.096	7.18	2.15	0.692	1.47	13.2	0.175	0.058	1.36
	15PGL0901-007(A)	0.121	0.573	4.10	0.617	2.49	1.23	0.241	0.006	2.13
	15PGL0901-007(B)	0.118	0.676	3.57	0.466	2.20	1.34	0.206	0.008	1.85
Standards	SDO-1	0.279	0.885	6.30	0.051	2.69	0.759	0.427	0.032	6.59
	SDO-1	0.266	0.876	6.47	0.043	2.80	0.764	0.407	0.032	6.50
	SBC-1	0.176	1.76	12.1	0.170	3.09	2.19	0.504	0.126	6.88
	SBC-1	0.158	1.56	11.0	0.178	2.92	2.08	0.499	0.116	6.57
	SGR-1b	2.29	2.48	3.21	0.130	1.32	5.81	0.154	0.025	2.10
	SGR-1b	2.35	2.84	3.50	0.143	1.34	5.95	0.162	0.027	2.20

5.2. Elemental and Mo isotope data for the oil and asphaltene separations

The elemental concentration and Mo isotope data for the oil and asphaltene separates are shown in **Table 7**. The V concentrations for two different digestions of standard crude oil NIST RM 8505 measured in this study were 384 ppm and 372 ppm, similar to the certified value of 390 ppm. The Mo concentrations were 0.201 ppm and 0.195 ppm. The δ^{98}Mo values of these two different digests (each measured three times during different analytical sessions) were 0.80 ± 0.04‰ (2SD; n = 3) and 0.81 ± 0.02‰ (2SD; n = 3). For comparison, Zhu (2017) obtained Mo concentrations of 0.230 ppm and δ^{98}Mo values of 0.78 ± 0.06‰ (2SD; n = 3) and 0.72 ± 0.03‰ (2SD; n = 3) using the same analytical protocol for NIST RM 8505. The four digests of NIST RM 8505 in this study and Zhu (2017) yield an overall average δ^{98}Mo of 0.78 ± 0.08‰ (2SD). A previously published average δ^{98}Mo of 0.51 ± 0.28‰ (n = 4; 2SD; re-normalized relative to NIST SRM 3134 = 0.25‰) was reported for NIST RM 8505 by Ventura et al. (2015). Our measurement of δ^{98}Mo thus overlaps that of Ventura et al. (2015) given 2SD uncertainties and is significantly more precise.

Compared with the source rocks, the crude oil samples have low Mo concentrations between 0.005 ppm and 0.392 ppm with an average of 0.159 ppm. Crude oil samples have V and Ni concentrations of 1.95-186 ppm (average = 55.9 ppm) and 0.533-50.5 ppm (average = 17.1 ppm), respectively. Each asphaltene sample has a higher Mo, V, and Ni concentration than its corresponding crude oil sample. The Mo, V, and Ni concentrations of the asphaltenes are 0.973-3.16 ppm (average = 1.89 ppm), 92.4-842 ppm (average = 485 ppm), and 20.3-245 ppm (average = 153 ppm), respectively.

Due to limited oil quantities and the low Mo concentrations in some crude oil and asphaltene samples, only fifteen crude oil and six asphaltene samples were measurable for Mo isotope compositions. Overall, the crude oil samples have δ^{98}Mo values of 0.53‰ to 1.53‰. Asphaltene samples have δ^{98}Mo values between 0.78‰ and 1.44‰. Crude oil samples have been divided into four groups according to the different reservoir effects shown in **Table 3**. The statistics for the elemental and Mo isotope data for the crude oils in these groups are shown in **Table 8**. Because of the narrow range of low Mo concentrations, the different crude oil groups do not exhibit significant differences in Mo concentration. However, lower δ^{98}Mo values are generally observed in crude oil samples that have been affected by TSR (0.53-1.23‰) and TSR + biodegradation + water washing (0.61-0.88‰) compared to samples not affected by reservoir effects (1.05-1.31‰) and samples affected only by biodegradation and water washing (0.92-1.53‰). Both the average and median δ^{98}Mo values are lower for the two crude oil groups affected by TSR. The V and Ni concentrations are also lower in the groups affected by TSR.

Table 7. Elemental and Mo isotope data for the crude oils and asphaltenes sourced from the Phosphoria Formation

	Sample Number	Sample Name	Mo[a] ppm	Mo[b] ppm	V ppm	Ni ppm	δ^{98}Mo ‰	2SD Measured	2SD Reported	n	δ^{34}S[a] ‰	Asphaltene Name
Crude Oil	1	408	0.298	0.336	186	50.5	1.53	0.01	0.11	3	-6.20	33102
	2	2063	0.170	0.143	63.6	19.9	1.09	0.07	0.11	3	-4.60	33106
	3	2078	0.029	0.038	31.2	8.71	1.17		0.11	1	-3.40	33107
	4	2077	0.009		16.7	3.83					-1.20	
	5	2085	0.180	0.333	902	23.0	1.50		0.11	1	-5.40	33104
	6	2076			34.0	11.3					1.70	
	7	2084	0.040	0.063	75.2	27.2	1.10	0.01	0.11	2	-4.70	
	8	3904	0.087	0.112	83.4	27.4	1.30	0.02	0.11	3	-4.00	33103
	9	2071	0.134	0.166	94.0	25.2	1.31	0.02	0.11	2	-4.70	33109
	10	3899	0.340	0.376	61.6	21.8	0.61	0.02	0.11	3	-0.90	
	11	3897	0.009	0.039	5.82	1.57	0.68	0.05	0.11	2	5.70	
	12	2709	0.145	0.155	33.9	13.1	1.23	0.01	0.11	3	0.30	33105
	13	2080			1.95	0.533					1.00	
	14	3672	0.392	0.458	45.2	15.2	0.53	0.01	0.11	3	4.10	
	15	3673	0.321	0.344	55.5	18.0	0.88	0.06	0.11	3	1.70	
	16	3674	0.381	0.416	69.0	22.9	0.87	0.01	0.11	3	1.90	33108
	17	2083	0.081	0.102	44.1	14.0	0.92	0.07	0.11	2	2.80	
	18	430	0.005		15.3	4.80					1.00	
	19	3895	0.076	0.081	56.4	16.2	1.05	0.07	0.11	3	-4.10	
Asphaltene		33102	1.85	0.897	842	226	0.788	0.05	0.11	3		
		33103	1.32	1.39	707	245	0.742	0.04	0.11	3		
		33104	2.33	2.47	617	195	0.760	0.01	0.11	3		
		33105	3.40	3.15	436	185	0.702	0.03	0.11	3		
		33106			92.4	20.3	0.820					
		33107			277	77.8	0.781					
		33108	1.70	1.83	327	108	0.752	0.01	0.11	3		
		33109	0.973	1.13	582	165	0.779	0.03	0.11	3		
Standards		NIST RM 8505	0.201	0.223	384	53.9	0.80	0.04	0.11	3		
		NIST RM 8505 (rpt)	0.195	0.223	372	53.2	0.81	0.02	0.11	3		
		NIST RM 8505[d]	0.230		400	55.0	0.78	0.06	0.11	3		
		NIST RM 8505[e]					0.72	0.03	0.11	3		

[a] Quadrupole calculated data with blank correction
[b] Double spike calculated data
[c] δ^{34}S data from Lillis and Selby (2013)
[d,e] data from Zhu (2017)

Table 8. The maximum, minimum, average, and median values for Mo, V, and Ni concentrations, and Mo isotope compositions for the crude oils affected by different reservoir effects

Reservoir Effect		No Reservoir effect	Biodegradation + Water washing	TSR	Biodegradation + Water washing + TSR
Mo (ppm)	Maximum	0.170	0.298	0.392	0.381
	Minimum	0.040	0.029	0.005	0.321
	Average	0.101	0.147	0.112	0.347
	Median	0.087	0.131	0.009	0.340
δ^{98}Mo (‰)	Maximum	1.31	1.53	1.23	0.88
	Minimum	1.05	0.92	0.53	0.61
	Average	1.17	1.43	0.81	0.79
	Median	1.10	1.33	0.68	0.87
V (ppm)	Maximum	94.0	186	45.2	69.0
	Minimum	56.4	31.2	1.95	34.0
	Average	74.5	87.8	19.8	55.0
	Median	75.2	67.1	16.0	58.6
Ni (ppm)	Maximum	27.4	50.5	15.2	22.8
	Minimum	16.2	8.71	0.532	11.3
	Average	23.2	24.0	6.50	18.5
	Median	25.2	18.5	4.32	19.9

6. Discussion

6.1. Elemental Concentration and Mo Isotope Constraints on Local Redox Conditions During Deposition of the Phosphoria Formation

To understand the Mo isotope compositions of petroleum source rocks and use this data to draw a general picture of global ocean redox conditions, interpreting local redox conditions and the degree of basin restriction from the open ocean is important. The Mo, V, and Zn concentrations, Mo/TOC ratios, and Mo/U ratios of the source rocks are useful geochemical tracers to constrain the local redox conditions and infer the degree of Phosphoria basin restriction from the open ocean by tectonic highlands (Maughan, 1994). It is necessary to know if the Phosphoria black shales and mudrocks were deposited under euxinic bottom water conditions because using the Mo isotope system to infer global redox conditions requires high dissolved H_2S (> 11 μM) and quantitative Mo removal from local bottom waters in the basin (Neubert et al., 2008; Algeo et al., 2010; Wignall et al., 2010; Zhou et al., 2012; Reubsam et al., 2017).

Vanadium hyper-enrichments (> 500 ppm) in black shales may be caused by a hyper-enrichment of H_2S in bottom waters (Scott et al., 2017). A recent study of the Bakken Shale and the lack of V hyper-enrichment in the most H_2S-rich euxinic basin in the modern ocean (Framvaren Fjord) led Scott et al. (2017) to suggest that V ≥ 500 ppm in black shales is a proxy for dissolved H_2S ≥ 8 mM in the water column. If the Zn concentration in sediments reaches 72-500 ppm, this primary authigenic enrichment is related to the enrichment of H_2S in the water column and in pore waters (Scott et al., 2017). Black shales with Zn concentrations ≥ 500 ppm may be caused by phototropic sulfide-oxidizing bacteria (PSOB) thriving in euxinic shallow waters within the photic zone (Scott et al., 2017). These bacteria produce polysulfides (S_x^{2-}) that

may complex with Zn and increase the efficiency of Zn removal from the water column (Scott et al., 2017).

Different geographic localities for Meade Peak Member deposition have different redox conditions that are indicated by Mo, V and Zn concentrations. Astoria samples from the Meade Peak Member have high Mo, V, and Zn enrichments and were likely deposited in a euxinic depositional environment based on their high Mo (52.2-443 ppm), V (485-6756 ppm), and Zn (770-1130 ppm) concentrations (cf. Scott and Lyon, 2012; Scott et al., 2017). Crystal Creek samples from the Meade Peak Member have low Mo (≤ 10 ppm) and V (39.2-198 ppm), but variable Zn (52.3-438 ppm) concentrations, which suggests H_2S was confined in sediment pore waters and that bottom waters were non-euxinic (Scott and Lyons, 2012; Scott et al., 2017). This implies different local redox conditions in each geographic locality. There are two samples (16PGL0914-06, 16PGL0914-07) with unusually high Mo and U EFs because these two samples are dolomitic to calcareous and have the lowest Al and highest Ca and Mg concentrations (**Table 6**). The Mo-TOC and Mo-U EF data for the euxinic Meade Peak Member in ***Figure 5*** and ***Figure 6*** are consistent with weak to moderate restriction of the Phosphoria Sea, which promoted more efficient Mo removal into the sediments compared with U. For the Astoria samples, the weakly to moderately restricted conditions combined with high H_2S levels (***Figure 5; Figure 6***) are suggested to have allowed pronounced enrichment of redox-sensitive elements in the sediment, but without quantitative element removal from the water column.

The Retort Member samples were deposited in non-euxinic to euxinic bottom waters but the magnitude of redox-sensitive metal enrichment could also be affected by other factors. Two Retort samples have Mo concentrations of 9.58-11.0 ppm and were likely deposited in a non-euxinic environment. These two samples plot lower on the Mo-U plot (***Figure 6***). The rest of the

Retort samples have high Zn (86.8-952 ppm), Mo (17.4-59.6 ppm) and V (53.0-327 ppm) concentrations. These shales have moderate Mo concentrations that suggest the depositional environment was either experiencing a strong degree of basin restriction or was intermittently euxinic (Scott and Lyon, 2012). In ***Figure 5*** and ***Figure 6***, the patterns of Mo-TOC and Mo-U EF data suggest euxinic conditions with a generally greater degree of basin restriction for the Retort Member depositional environment compared to that of the Meade Peak Member. The strong basin restriction limited water exchange and thus the rate of element recharge from the open ocean, resulting in a low enrichment of Mo and V in the sediments. High Zn concentrations (>500 ppm) in the Retort Member might be caused by phototropic sulfide-oxidizing bacteria (PSOB) thriving in euxinic shallow waters within the photic zone (Scott et al., 2017). Lower Zn concentrations (<500 ppm) represent less reducing conditions but with enrichment of H_2S in water column and/or pore waters (Scott et al., 2017).

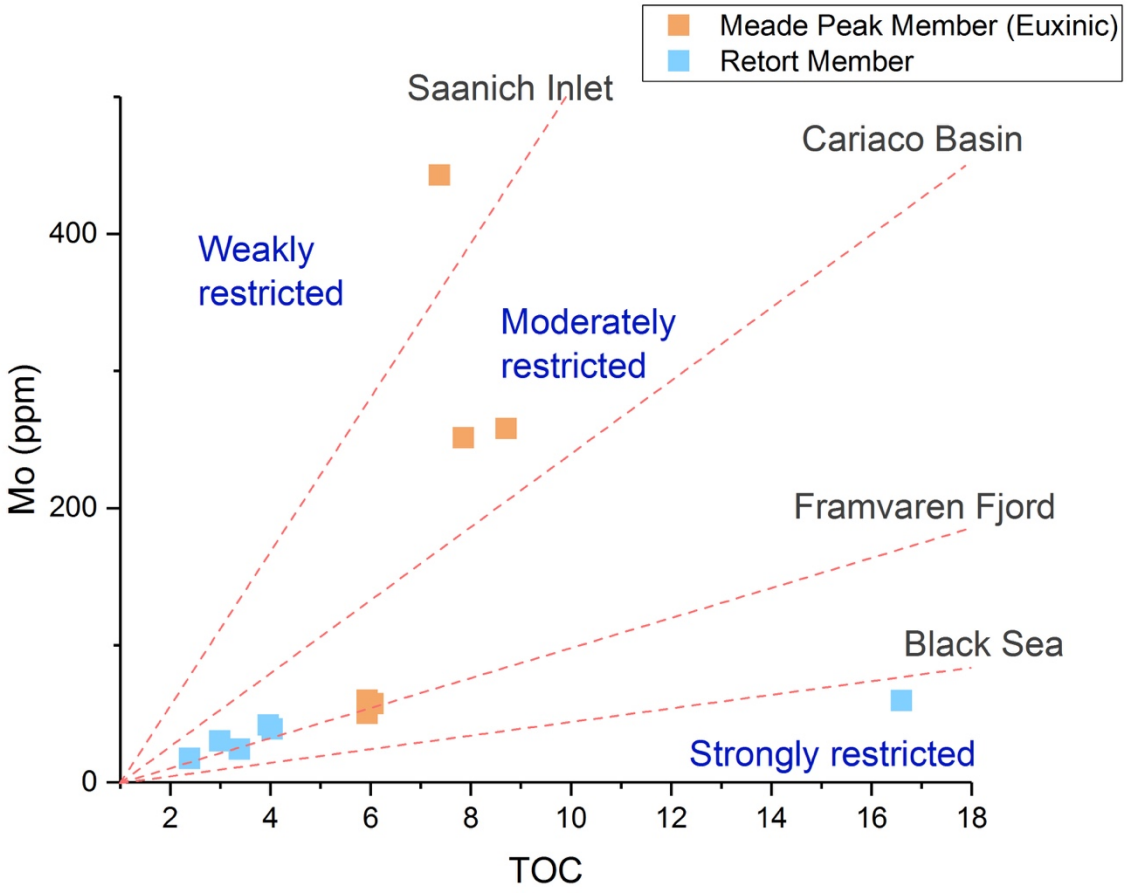

Figure 5. Geological diagrams showing Mo concentrations versus TOC. Dashed lines represent regression slopes for four modern anoxic basins: Saanich Inlet: 45 ± 5 ppm/wt%; Cariaco Basin: 25 ± 5 ppm/wt%; Framvaren Fjord: 9 ± 2 ppm/wt%; Black Sea: 4.5 ± 1 ppm/wt% (Algeo and Lyons, 2006).

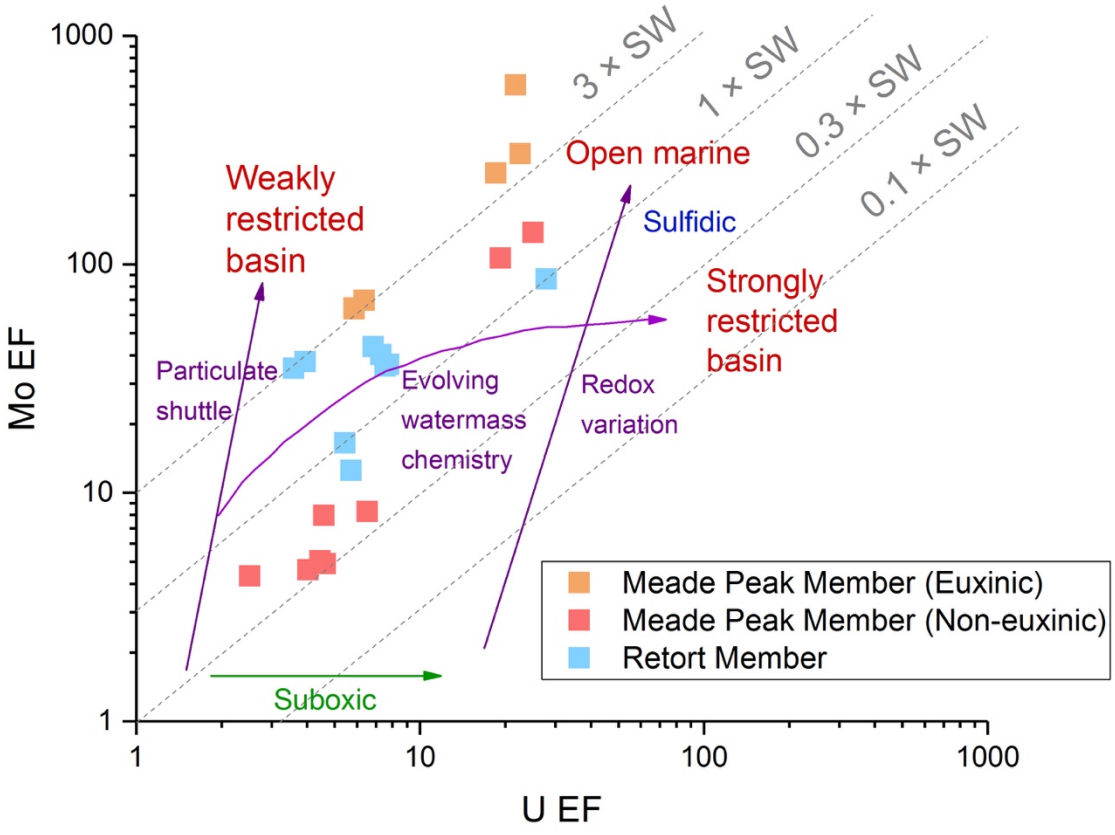

Figure 6. Geochemical diagrams showing Mo EF vs U EF. Dash lines represent the molar Mo/U ratios of modern seawater, and their corresponding fractions of modern seawater (1 × SW; 0.1 × SW; 0.3 × SW; 3 × SW; Algeo and Tribovillard, 2009). The model of Mo-U enrichment patterns and their corresponding controls are from Algeo and Tribovillard (2009).

The Mo isotope compositions of Phosphoria black shales have a range of 0.37-2.27‰ and an average of 1.27‰ (2SD = 0.53‰), which is lower than the modern seawater composition (2.34 ± 0.10 ‰; Barling et al., 2001; Siebert et al., 2003; Nakagawa et al., 2012; Nägler et al., 2014). The average δ^{98}Mo in the euxinic Meade Peak Member, non-euxinic Meade Peak Member, euxinic Retort Member, and non-euxinic Retort Member are 1.62‰ (2SD = 0.15‰), 0.80‰ (2SD = 0.61‰), 1.56‰ (2SD = 0.24‰), and 1.06‰ (2SD = 0.01‰), respectively. For

both the Retort Member and Meade Peak Member, those mudrocks inferred to be deposited from non-euxinic bottom waters (based on the elemental data) typically have lower δ^{98}Mo compared to those mudrocks inferred to be deposited from euxinic bottom waters. The elemental and Mo isotope data are thus consistent with regards to local bottom water redox conditions.

If there was quantitative removal of Mo from bottom waters into sediments, then the Mo isotope compositions from euxinic black shales may represent the coeval seawater compositions. If $[H_2S]_{aq} < 11$ μmol, the quantitative conversion of molybdate to highly particle-reactive tetrathiomolybdate is not likely and the removal of Mo from bottom waters would not become quantitative. If $[H_2S]_{aq} > 11$ μmol, but Mo removal is still not quantitative due to a high rate of Mo recharge to bottom waters of less restricted basins, then Mo isotope fractionation between seawater and sediments may be around 0.5 ‰ (Nagler et al., 2011). In the non-euxinic Meade Peak Member and the euxinic Retort Member, there are poor correlations between δ^{98}Mo and Mo concentrations ($R^2 = 0.22$; $R^2 = 0.14$, respectively; ***Figure 7***). The negative correlation (***Figure 7***; $R^2 = 0.89$) shown in the euxinic Meade Peak Member may be caused by the non-quantitative removal of Mo from bottom waters with $[H_2S]_{aq} >> 11$ μmol (based on the high V and Zn concentrations; cf. Scott et al., 2017). The weak to moderate basin restriction would also result in non-quantitative Mo removal into sediments due to significant Mo recharge from open ocean to the bottom water in the Phosphoria basin. This may cause a 0.5‰ Mo isotope fractionation between sediments and the strongly euxinic bottom waters (Nagler et al., 2011). Any expression of Mo isotope fractionation between sediments and seawater results in preferential removal of isotopically lighter Mo isotopes to sediments (Kendall et al., 2017 and references therein). So, the highest Mo isotope composition of 1.77‰ for the euxinic Meade Peak Member would represent the minimum value for the coeval global seawater Mo isotope

composition at ca. 270 Ma. Similarly, the highest Mo isotope composition of 1.98‰ in the Retort Member is the minimum Mo isotope composition of coeval global seawater at ca. 265 Ma.

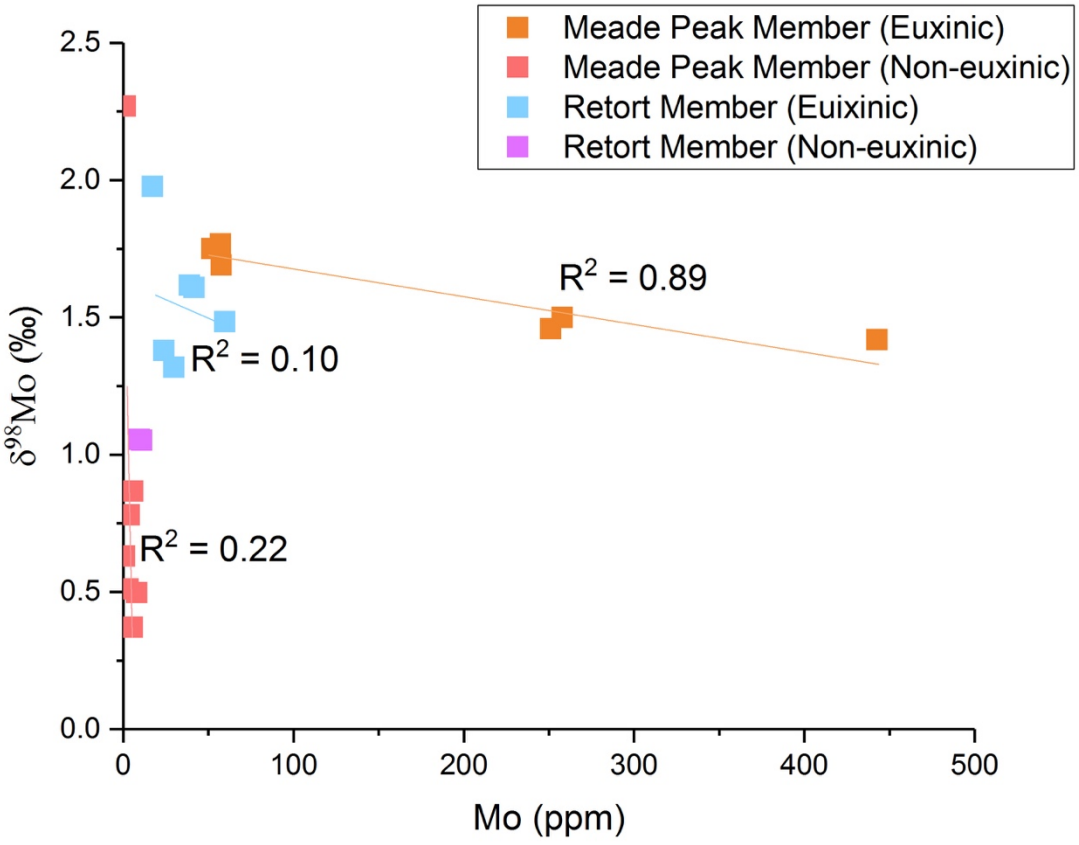

Figure 7. Geochemical diagram showing the relationship between Mo (ppm) and δ^{98}Mo in euxinic and non-euxinic Phosphoria Formation mudrocks.

6.2. Mo partitioning in oils

Mo concentrations in Phosphoria crude oil have a range of 0.005 ppm to 0.392 ppm, which is significantly lower than the average upper crustal Mo abundance of 1.5 ppm (McLennan, 2001). This observation suggests that little Mo was transferred from TOC-rich (≥

2.39 wt%) Phosphoria source rock (Mo content: 9.58-443 ppm) to crude oil in the Phosphoria petroleum system. These low values are consistent with the measured crude oils sourced from Phanerozoic aged sedimentary basins in Russia, Kuwait, USA, Venezuela, and Brazil, which have Mo concentrations of 0.01-0.39 ppm except for one crude oil that has a Mo concentration of 1.44 ppm (Ventura et al., 2015). Molybdenum concentrations in Phosphoria asphaltene (0.973-3.16 ppm) are higher compared with their associated bulk crude oils, which suggests a significant portion of the Mo in oils is likely concentrated in the asphaltene fraction. A significant enrichment of V and Ni in the asphaltene component, relative to the crude oils, is also observed.

Scatter is observed when comparing the Mo, V, and Ni abundances in bulk crude oil versus its asphaltene fraction (***Figure 8***). There is no strong positive correlation for Mo, V, and Ni abundances between crude oils and asphaltenes, in contrast with the significant positive correlation for Re and Os concentrations in bulk crude oils and asphaltenes for other petroleum systems (Selby et al., 2007). Since Re and Os have a strong positive correlation between the oil and asphaltene, Re and Os concentrations in the asphaltene fraction increase with the concentrations in the bulk crude oil, and thus the asphaltene fraction can be treated as being representative of the whole oil. However, in this study, significant correlation for elements in the whole oil and asphaltene are not observed, so the asphaltene separates cannot be used to represent the whole oil. The asphaltene might not be the only major host for Mo, V, and Ni in the Phosphoria crude oils. Vanadium and nickel might be stored in porphyrins in aromatic and resin fractions of oils.

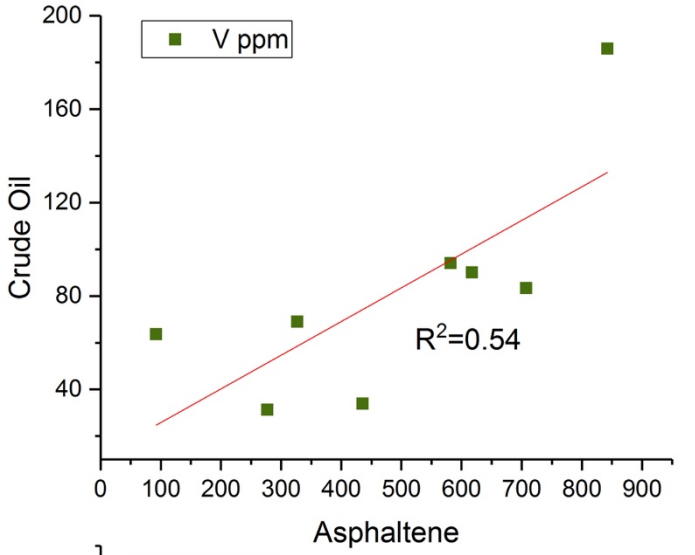
V ppm
Crude Oil
Asphaltene
R^2=0.54
200
160
120
80
40
0
100
200
300
400
500
600
700
800
900

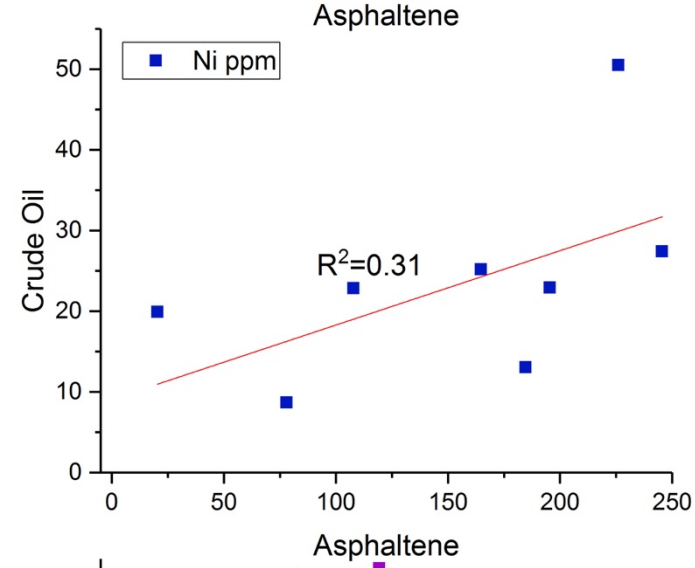
Ni ppm
Crude Oil
Asphaltene
R^2=0.31
50
40
30
20
10
0
0
50
100
150
200
250

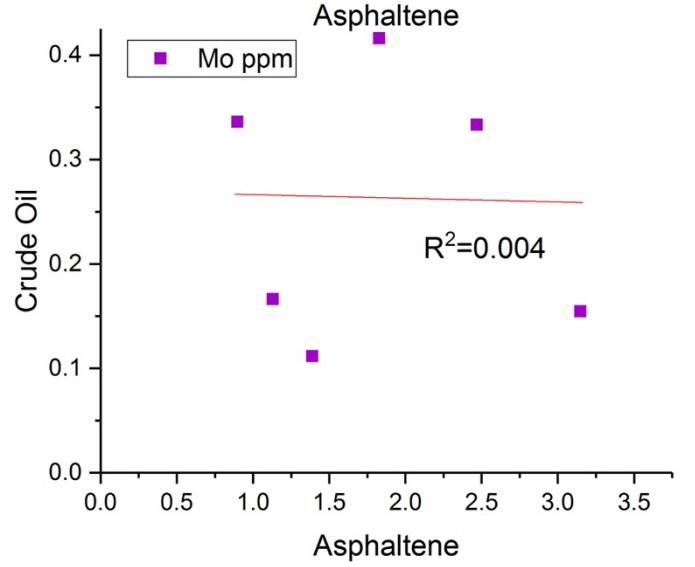
Mo ppm
Crude Oil
Asphaltene
R^2=0.004
0.4
0.3
0.2
0.1
0.0
0.0
0.5
1.0
1.5
2.0
2.5
3.0
3.5

Figure 8. Mo, V, and Ni abundances (ppm) in crude oil versus the Mo, V, Ni abundances (ppm) in asphaltene extracted from the whole oil.

If the asphaltene fraction is the major host of Mo in the crude oil, then the asphaltene Mo isotope composition will exert a major control on the bulk oil Mo isotope composition. In general, the crude oil samples have δ^{98}Mo values of 0.53‰ to 1.53‰. Asphaltene samples have δ^{98}Mo values between 0.78‰ and 1.44‰, and have a mild positive correlation with the bulk crude oil δ^{98}Mo values (***Figure 9***; $R^2 = 0.47$). In five of six samples, the δ^{98}Mo value is generally higher for the crude oil than the corresponding asphaltene separate. The isotopic offsets between the crude oil and asphaltene of each sample are -0.088‰, -0.329‰, -0.191‰, -0.296‰, 0.120‰, and -0.093‰. If the long-term analytical uncertainty for Mo isotopes of 0.11‰ is taken into consideration, the δ^{98}Mo value of each crude oil is equal to or only slightly higher than its asphaltene fraction. For those samples where the asphaltene Mo isotope composition is lower than the crude oil, it suggests other fractions of the oil might have a higher Mo isotope composition than the bulk crude oil and asphaltene. Alternatively, the process of separating asphaltene from the crude oil caused Mo isotope fractionation.

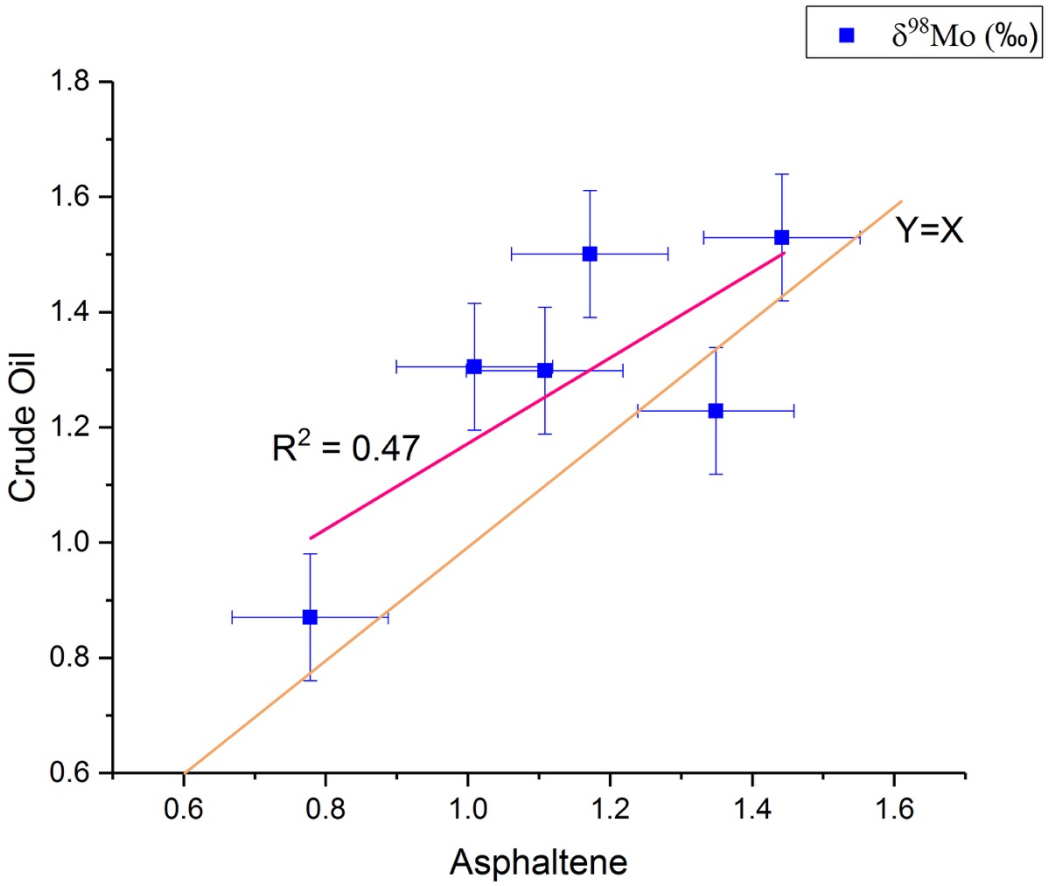

Figure 9. Comparison of δ^{98}Mo compositions (‰) in crude oils and their asphaltene fraction

6.3. Potential to use Mo isotope compositions to correlate black shales and oils

Black shales deposited under a strongly euxinic environment with high TOC have significant potential for generating oil. Moreover, the black shales with the highest TOC and Mo contents are the most representative of the source rocks that could have transferred Mo to the Phosphoria oils. The Meade Peak Member and Retort Member mudrocks with 2.4-16.6 wt% TOC, deposited primarily from euxinic bottom waters, are best for analyzing the relationship between oil and its sourced rock. Although most mudrock samples analyzed in this study are thermally mature to overmature, their Mo concentration and isotope data likely reflect depositional conditions because the orders of magnitude lower Mo concentrations in oils versus the most Mo- and TOC-rich mudrocks indicates that the Mo mass balance is probably dominated by the source rocks during oil generation.

In general, different organic-rich mudrocks have different Mo isotope signatures. If there are Mo isotope correlations between the oil-source rock and oil, then the Mo isotope composition of oils can be used to fingerprint the major oil source rock. In the Phosphoria Formation, there is an overlap of Mo isotope composition between the two shale members. The Retort Member samples have Mo isotope compositions of 1.05‰ to 1.98‰, whereas the euxinic Meade Peak Member samples have Mo isotope compositions of 1.42‰ to 1.77‰ (***Figure 10***). Oils affected by reservoir processes are not relevant to discussing oil-source correlation, as only oils not affected by reservoir processes and euxinic black shales should be compared. Except for the two low-Mo and low-TOC Retort samples (δ^{98}Mo = 1.05‰ and 1.06‰) deposited from non-euxinic bottom waters, the Mo isotope data of the other TOC-rich Phosphoria Formation mudrocks (likely deposited from euxinic bottom waters) are higher than those of the unaltered oils (1.05-

1.31‰). Hence, it is not possible to correlate the Mo isotope compositions of oils with a specific source rock member from the Phosphoria Formation.

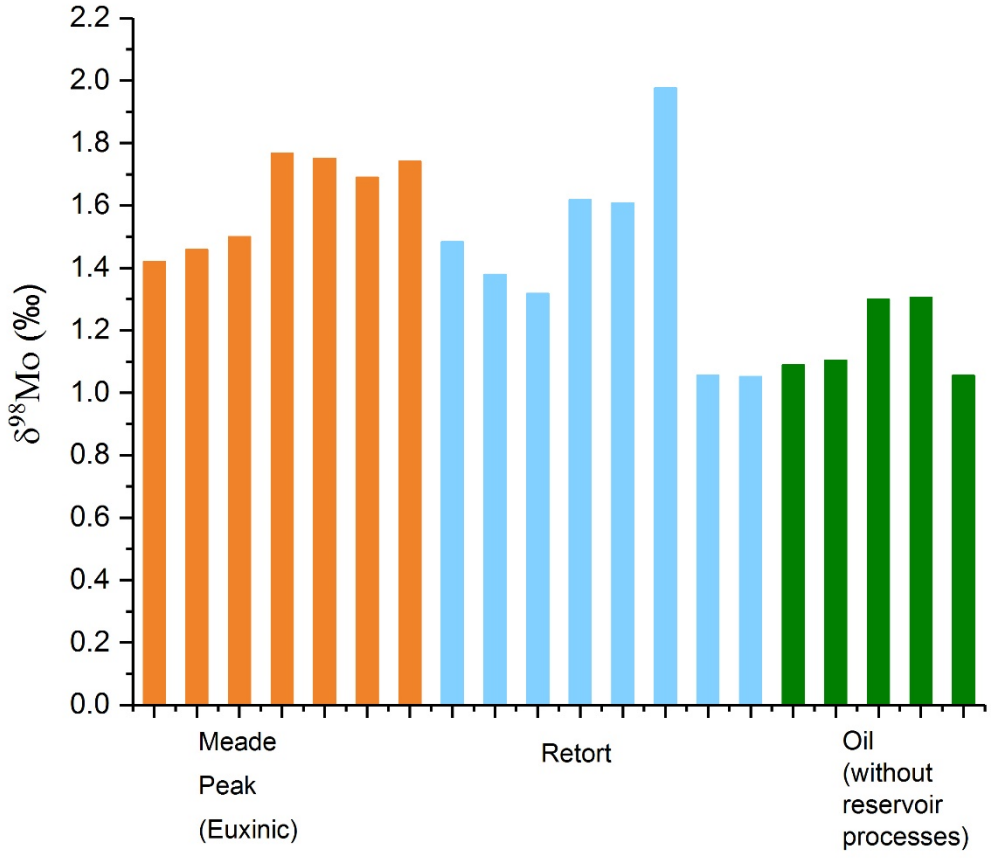

Figure 10. Comparison of Mo isotope compositions in oils (minimally affected by reservoir processes) and the TOC-rich (> 2.4 wt%) Phosphoria Formation mudrocks.

The low Mo concentrations of the oils makes the Mo isotope composition of the oil susceptible to modification. Along the migration pathway, the oil may have interacted with waters and rocks containing isotopically lighter Mo, resulting in a decrease in the Mo isotope composition of the oil. It is also possible that Mo isotope fractionation during oil generation caused isotopically light Mo to be released preferentially from shales to the oil.

6.4. Evaluation of reservoir effects on Mo isotope compositions of Phosphoria oils

6.4.1. Effects of biodegradation and water washing

Five crude oil samples (2, 7, 8, 9, 19) are minimally affected by reservoir processes, allowing a comparison of the δ^{98}Mo from these samples with crude oil samples affected to various extents by TSR, biodegradation, and water washing. This comparison aims to determine the influence of reservoir processes on Mo isotope compositions in oils. The Mo isotope compositions in crude oil minimally affected by reservoir processes is 1.05-1.31‰ ***(Figure 11).***

There may be a slight increase in the δ^{98}Mo of oil samples that were affected only by biodegradation and water washing and not TSR. Of these four crude oil samples, two of them have higher δ^{98}Mo (around 1.5‰) than minimally altered oil samples. However, one sample has similar δ^{98}Mo (around 1.1‰) as the minimally altered oil samples and one sample has lower δ^{98}Mo (0.92‰). So, there is no obvious biodegradation and water washing effect on crude oil δ^{98}Mo compositions.

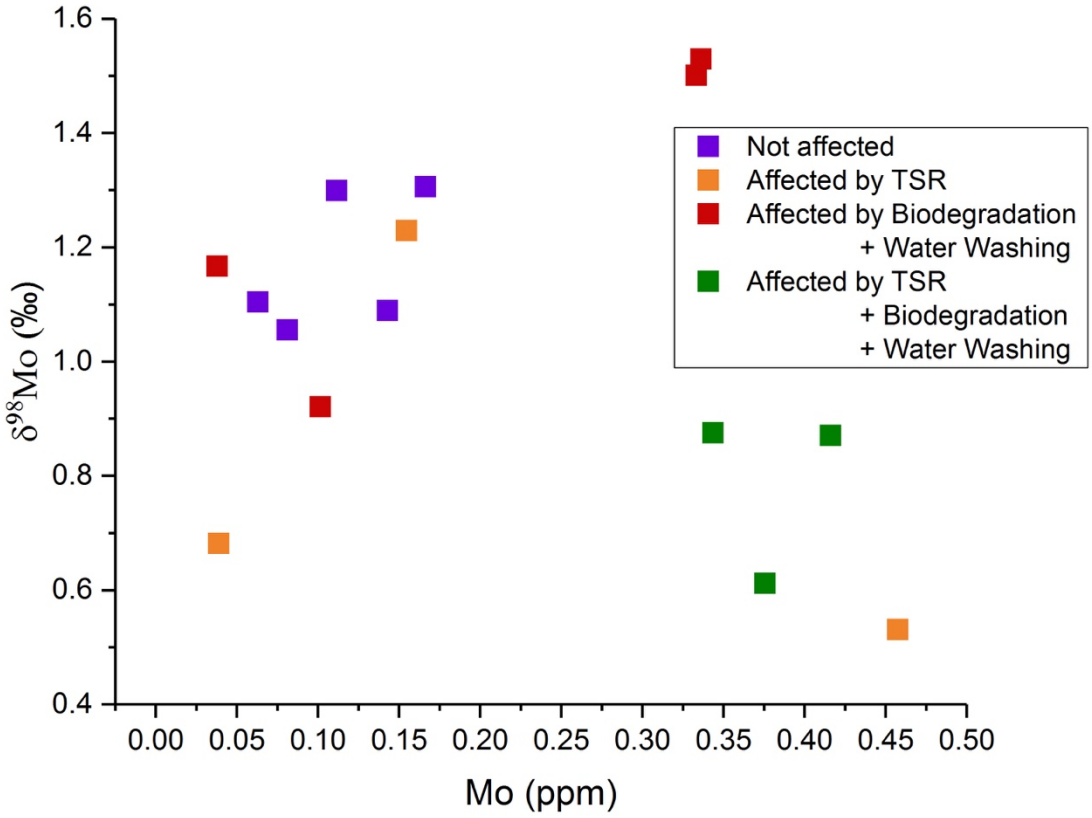

Figure 11. δ^{98}Mo values and Mo concentrations of crude oil samples affected by different reservoir processes (TSR, biodegradation + water washing, TSR + biodegradation + water washing) and comparison with minimally altered crude oils.

6.4.2. Effects of thermochemical sulfate reduction

Redox reactions commonly occur between hydrocarbons or other organic compounds and sulfate in petroleum reservoirs at elevated temperatures where there is anhydrite or other sources of sulfate (Goldstein and Aizenshtat, 1994; Machel et al., 1995; Lillis and Selby, 2013). Such redox reactions result in sulfate being reduced to sulfide, and petroleum is oxidized to carbon dioxide (CO_2) inorganically, producing primary and secondary products such as carbonate minerals, solid bitumen, metal sulfides and other organosulfur compounds (Goldstein and Aizenshtat, 1994; Machel et al., 1995; Lillis and Selby, 2013). The onset temperature of TSR in

the Phosphoria petroleum system is about 100°C but the minimum temperature depends on a number of factors such as oil composition, reservoir environment, and availability of sulfate (Orr, 1974; Goldhaber and Orr, 1995; Worden et al., 1995; Machel, 2001; Lillis and Selby, 2013). Metal isotope compositions may be affected by TSR, which has been verified to cause scatter in Re-Os isotope systematics on a Re-Os isochron diagram, thus precluding the determination of a Re-Os oil generation age (Lillis and Selby, 2013).

Based on the TAS values listed in **Table 2**, the thermal maturity trend for the Phosphoria oils is shown in ***Figure 12***. There is a moderate correlation ($R^2 = 0.47$) between the thermal maturity and δ^{98}Mo of non-TSR altered oils. Decreasing δ^{98}Mo in crude oil is associated with higher thermal maturity of the oil.

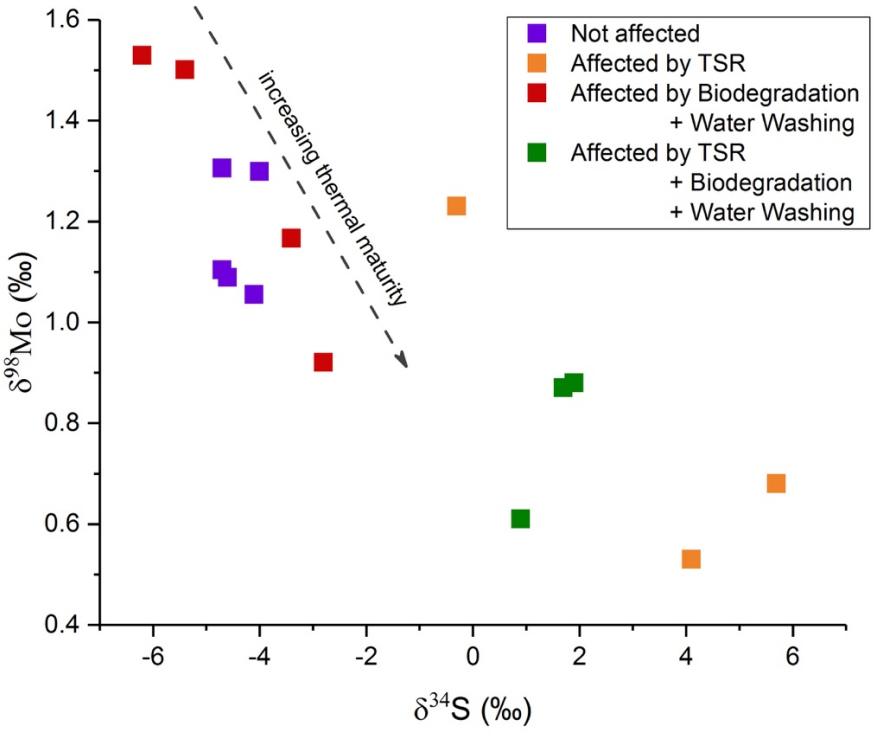

Figure 12. δ^{98}Mo versus δ^{34}S in crude oils, showing a decrease in the isotopic composition of both elements for oils affected by TSR and for oils with increasing thermal maturity.

The Phosphoria crude oils that were influenced by TSR have generally lower Mo isotope compositions compared with the crude oils and asphaltenes that were not affected by TSR (***Figure 12***). The Mo isotope compositions in crude oil that were minimally affected by reservoir processes are 1.05-1.31‰. Three crude oil samples affected only by TSR have a range in Mo isotope compositions of 0.53-1.23‰ (sample 11, 12, 14). Crude oils with higher $\delta^{34}S$ indicates a greater influence of TSR on oil geochemistry. Samples 11 and 14 have relatively high $\delta^{34}S$ values of 5.7‰ and 4.1‰, respectively, and the $\delta^{98}Mo$ of these two samples are 0.68‰ and 0.53‰, respectively. Compared with sample 12 ($\delta^{34}S$ = -0.3‰; $\delta^{98}Mo$ = 1.23‰), samples 11 and 14 have a more severe TSR influence and lower $\delta^{98}Mo$. Another three crude oil samples (samples 10, 15, 16) that are affected by all three reservoir processes (biodegradation, water washing, TSR) have Mo isotope compositions of 0.61-0.88‰. Considering the inconspicuous effect of biodegradation and water washing on crude oil discussed earlier, TSR has likely also caused a decrease in the $\delta^{98}Mo$ of these crude oils.

There are two possible reasons to explain why there are low $\delta^{98}Mo$ values in TSR-altered oils. If molybdate-bearing fluids migrated into the oil reservoir, the Mo isotope signatures of oils may have become lighter than the initial Mo isotope composition of the oils as a result of the TSR reaction. Specifically, the reaction between H_2S and molybdate (MoO_4^{2-}) may have produced isotopically light thiomolybdates and possibly Mo-Fe-S phases (Zheng et al., 2000). However, if all molybdate entering the oil reservoir was transformed to thiomolybdate, then the added Mo will carry the isotopic signature of the molybdate introduced into the oil reservoir.

A negative correlation between $\delta^{34}S$ and $\delta^{98}Mo$ in TSR-altered oils is observed in ***Figure 12***. The higher $\delta^{34}S$ for TSR-altered oils was due to isotopically heavy S from evaporates being introduced into the oil reservoir. The most likely reason to explain the lower $\delta^{98}Mo$ values in

TSR-altered oils is that isotopically light molybdates were introduced into the oil reservoir, thus causing a decrease in the δ^{98}Mo of the oil.

6.5. Mo isotope constraints on Permian global seawater redox conditions

The Mo isotope compositions of the Phosphoria black shales have a range of 0.37-2.27‰, and an average of 1.27‰ (2SD = 0.53‰), which is lower than the modern seawater isotope composition (2.34 ± 0.10‰; Barling et al., 2001; Siebert et al., 2003; Nakagawa et al., 2012; Nägler et al., 2014). Specifically, the average δ^{98}Mo in the euxinic Meade Peak Member, non-euxinic Meade Peak Member, euxinic Retort Member, and non-euxinic Retort Member are 1.62‰ (2SD = 0.15‰), 0.80‰ (2SD = 0.61‰), 1.56‰ (2SD = 0.24‰), and 1.06‰ (2SD = 0.01‰), respectively. If there was quantitative removal of Mo from bottom waters into sediments, then the Mo isotope compositions from euxinic black shales may represent the coeval seawater compositions. If $[H_2S]_{aq} < 11$ μM, the quantitative formation of highly particle-reactive tetrathiomolybdate is not likely and hence quantitative removal of Mo from bottom waters is also not likely. The fractionation factor between seawater and modern weakly euxinic sediments (bottom water $[H_2S]_{aq} < 11$ μM) ranges widely from 0.5‰ to 3‰ (Arnold et al., 2004; Neubert et al., 2008). If $[H_2S]_{aq} > 11$ μM, Mo removal is still not quantitative due to a high rate of Mo recharge to bottom waters in less restricted basins, and hence the Mo isotope fractionation between seawater and sediments may be around 0.5 ‰ (Nagler et al., 2011). So, the highest value in euxinic sediments conservatively represents the minimum δ^{98}Mo value of the coeval seawater. The mudrock samples from the Phosphoria Formation that were deposited in a non-euxinic environment likely do not capture the seawater δ^{98}Mo signature.

The highest δ^{98}Mo values in the euxinic Meade Peak Member and Retort Member are 1.77‰ and 1.98‰, respectively. Considering the Mo isotope fractionation, these would be the minimum Mo isotope compositions of coeval global seawater. Comparing these values with the modern well-oxygenated seawater δ^{98}Mo of 2.34‰, both of the highest Mo isotope compositions from the two Phosphoria Formation members point to a generally well-oxygenated global ocean at ca. 270 Ma and 265 Ma, ~13-18 Myr before the greatest Phanerozoic mass extinction event in the Late Permian.

Other previous studies reported δ^{98}Mo and δ^{238}U compositions in Late Permian black shales, and give evidence for globally well-oxygenated seawater at the end of Permian before the mass extinction. The Late Permian Dalong Formation has highest δ^{98}Mo values of about 2‰ (Zhou et al., 2012). Comparing this value with the modern ocean δ^{98}Mo of 2.34‰, this implies generally well-oxygenated seawater at the end of Permian before the mass extinction (Zhou et al., 2012).

The δ^{238}U has also been measured to interpret the ocean redox conditions in the Late Permian before, during, and after the mass extinction (Brennecka et al., 2011; Lau et al., 2016; Elrick et al., 2017). A great proportion of the isotopically heavy U in seawater was sequestered into anoxic sediments that covered a large area of seafloor when there was a global ocean anoxic event (Andersen et al., 2014). Consequently, global seawater shifts to lighter δ^{238}U during times of expanded ocean anoxia compared to the modern predominantly well-oxygenated ocean where anoxic sediments are confined to oxygen minimum zones along productive ocean margins and in restricted basins. High δ^{238}U in carbonate rocks represents a predominantly well-oxygenated global ocean redox state (like today), whereas low δ^{238}U can be interpreted as evidence for extensive global ocean anoxia. The δ^{238}U of the modern ocean is -0.39 ± 0.02‰ (2SD; Stirling et

al., 2007; Weyer et al., 2008; Noordmann et al., 2016). The $\delta^{238}U$ in Middle to Late Permian carbonates (259-252 Ma) were measured in the Daxiakou section of South China (Elrick et al., 2017). The Middle and Late Permian ocean (259-252 Ma) have broadly the same redox conditions as that of modern ocean because the $\delta^{238}U$ values of the carbonates are close to that of modern seawater (Elrick et al., 2017). The Phosphoria Formation Mo isotope data, together with the carbonate U isotope data, suggests that a globally well-oxygenated ocean redox state characterized the Permian in the nearly ~20 Myr prior to the mass extinction. Increasingly oxygenated conditions (to levels possibly greater than that of the modern ocean) may have occurred in the ~ 2 Myr prior to the end-Permian mass extinction event (Elrick et al., 2017). An abrupt decrease of about 0.30‰ in the $\delta^{238}U$ values of carbonates across the end-Permian extinction horizon (252 Ma) has been observed in the Dajiang, Dawen, and Guandao sections in southern China (Brennecka et al., 2011; Lau et al., 2016), and an abrupt negative shift of >0.50‰ of $\delta^{238}U$ was also observed in the Daxiakou section at ca. 252 Ma, which all indicate a significant oceanic anoxia event associated with the mass extinction (Elrick et al., 2017). Between 251.9 Ma and 247.2 Ma (end-Permian and earliest Triassic, U isotope data from carbonates coupled with mass-balance modelling suggest that there were multiple episodes of expanded ocean anoxia (with anoxic waters covering between 12% and 65% of the seafloor) that were associated with peaks in the rate of biological extinction (Lau et al., 2016; Zhang et al., 2018).

7. Conclusions

In this study, the Mo isotope systematics of the Phosphoria petroleum system, Bighorn Basin, U.S.A., are explored in detail for the first time. This study reported the elemental concentrations and Mo isotope compositions for the black shale source rocks, crude oils, and asphaltene fractions of the crude oils. An improved approach to digest oils and asphaltenes was developed to obtain precise and accurate Mo isotope data.

Through the analysis of Mo, V, and Ni concentrations in Phosphoria black shales, both the Meade Peak Member and Retort Member mudrocks were deposited from both euxinic and non-euxinic conditions, consistent with previous studies (e.g., Hiatt and Budd, 2003). The patterns of Mo/TOC ratios and Mo/U ratios suggest that the Meade Peak Member was deposited in a weakly to moderately restricted basin, whereas the Retort Member was generally deposited in a more strongly restricted basin.

Elemental and isotope data in both crude oils and asphaltenes were measured in this study. Mo concentrations in the asphaltenes have a range of 0.973–3.16 ppm, which are higher compared with the bulk crude oils (0.055–0.392 ppm). Hence, asphaltenes are a major host of Mo in crude oils. However, Mo concentrations in both the bulk oils and asphaltenes are much lower than in the Phosphoria Formation organic-rich mudrocks (up to hundreds of ppm). So, Mo has not efficiently transferred to oil from the kerogen in the source rocks. V and Ni transfer from black shale into oils to a greater extent than Mo. It is likely that there are other important organic hosts in crude oils (e.g., aromatics and resins) that may store Mo. The δ^{98}Mo of some asphaltene samples are lower than that of crude oil, so there might be one or more fractions of oil with higher Mo isotope signatures than asphaltene and the bulk oil.

The Mo isotope signatures of black shales with high TOC and Mo content (indicative of a euxinic depositional environment) are most relevant for assessing oil and source rock correlation. However, the euxinic Meade Peak Member and euxinic Retort Member have overlapping Mo isotope compositions. So, it is not straightforward to establish which of these two units is the main source rock for the Phosphoria oil based on Mo isotopes. The Mo isotope compositions of the crude oils minimally altered by reservoir effects are 1.05-1.31‰, most of which are lower than those of the euxinic Meade Peak Member (1.42-1.77‰) and the largely euxinic Retort Member (1.05-1.98‰). This observation may reflect Mo isotopic fractionation at the time of oil generation and during oil migration, for example, oil may have interacted with formation waters/rocks and trapped isotopically light Mo from them, causing a lower Mo isotope signature in the oil. If correct, Mo isotopes may not be useful for oil-source rock correlation.

The effect of thermochemical sulfate reduction, biodegradation, and water washing on oil reservoirs has been studied. Thermochemical sulfate reduction has a significant effect, causing a decrease in the δ^{98}Mo compositions of oil. The Mo isotope compositions in crude oil without reservoir processes are 1.05-1.31‰. Crude oil samples affected by TSR have generally lower δ^{98}Mo of 0.53-1.23‰ (most TSR-altered oil samples have δ^{98}Mo <0.9‰). These lower values could be explained by introduction of fluids that contain isotopically light Mo into the oil. Water washing and biodegradation do not have a clear effect on the δ^{98}Mo of crude oils.

The highest Mo isotope composition of euxinic sediments and black shales represents the most conservative estimate for the global seawater Mo isotope composition at the time of deposition, because any Mo isotope fractionation between seawater and sediments results in preferential removal of lighter Mo isotopes to the sediment. Combining this observation with the Mo isotope values in the Phosphoria black shales, the highest Mo isotope composition of 1.77‰

from the euxinic Meade Peak Member and 1.98‰ from the Retort Member represent the minimum values for coeval seawater at ca. 270 and ca. 265 Ma, respectively. These values, close to the modern seawater Mo isotope composition of 2.34‰, suggest an extensively oxygenated global ocean. Together with other Mo and U isotope data from sedimentary rocks, extensively well-oxygenated oceans (broadly similar to today) may have prevailed in the nearly ~20 Myr before the greatest animal extinction event during the latest Permian.

Despite the significant advances made regarding Mo isotope systematics in petroleum systems in this study, there is still significant opportunity for future work that needs to be done. 1) Due to the limitation of the volume of oil and asphaltene samples, Mo isotope data could not be obtained for all samples. Future studies could collect more oil and asphaltene samples with enough volume, allowing a more comprehensive study on the Mo isotope system in the Phosphoria petroleum system. 2) Elemental concentrations and isotope data from other fractions in the oil besides asphaltene could be measured to compare with those of asphaltene and the bulk oil, thereby establishing a more complete Mo isotopic mass balance for crude oils and identify the major hosts of Mo in oil. 3) Hydrous pyrolysis experiments are needed to study Mo isotope fractionation upon generation of the oil. 4) The effect of formation waters on the Mo isotope composition of oils during oil migration needs to be tested.

8. References

Algeo, T. J., Hinnov, L., Moser, J., Maynard, J. B., Elswick, E., Kuwahara, K., & Sano, H. (2010). Changes in productivity and redox conditions in the Panthalassic Ocean during the latest Permian. Geology, 38(2), 187-190.

Algeo, T. J., Kuwahara, K., Sano, H., Bates, S., Lyons, T., Elswick, E., ... & Maynard, J. B. (2011). Spatial variation in sediment fluxes, redox conditions, and productivity in the Permian–Triassic Panthalassic Ocean.Palaeogeography, Palaeoclimatology, Palaeoecology, 308(1), 65-83.

Algeo, T. J., & Lyons, T. W. (2006). Mo–total organic carbon covariation in modern anoxic marine environments: Implications for analysis of paleoredox and paleohydrographic conditions. Paleoceanography, 21(1).

Algeo, T. J., & Tribovillard, N. (2009). Environmental analysis of paleoceanographic systems based on molybdenum–uranium covariation.Chemical Geology, 268(3), 211-225.

Archer, C., & Vance, D. (2008). The isotopic signature of the global riverine molybdenum flux and anoxia in the ancient oceans. Nature Geoscience, 1(9), 597-600.

Archer, C., Elliott, T., van den Boorn, S., and van Bergen P., Mo and Ni Isotope Systematics in Petroleum Fluids Across Subsurface Alteration Gradients. Mineralogical Magazine, 2012, Volume 76, 1433.

Arnold, G. L., Anbar, A. D., Barling, J., & Lyons, T. W. (2004). Molybdenum isotope evidence for widespread anoxia in mid-Proterozoic oceans. Science,304(5667), 87-90.

Andersen, M. B., Stirling, C. H., & Weyer, S. (2017). Uranium isotope fractionation. Reviews in Mineralogy and Geochemistry, 82(1), 799-850.

Barbat, W. N. (1967). Crude-oil correlations and their role in exploration. AAPG Bulletin, 51(7), 1255-1292.

Baker, E.W. (1969) In: Organic Geochemistry, G. Eglinton and M.T.J. Murphy (eds.), Springer-Verlag, New York.

Barling, J., Arnold, G. L., & Anbar, A. D. (2001). Natural mass-dependent variations in the isotopic composition of molybdenum. Earth and Planetary Science Letters, 193(3), 447-457.

Barling, J., & Anbar, A. D. (2004). Molybdenum isotope fractionation during adsorption by manganese oxides. Earth and Planetary Science Letters, 217(3), 315-329.

Barwise, A. J. G. (1990). Role of nickel and vanadium in petroleum classification. Energy & Fuels, 4(6), 647-652.

Benton, M. J., & Twitchett, R. J. (2003). How to kill (almost) all life: the end-Permian extinction event. Trends in Ecology & Evolution, 18(7), 358-365.

Brennecka, G. A., Herrmann, A. D., Algeo, T. J., & Anbar, A. D. (2011). Rapid expansion of oceanic anoxia immediately before the end-Permian mass extinction. Proceedings of the National Academy of Sciences, 108(43), 17631-17634.

Campbell, C. V. (1962). Depositional environments of Phosphoria Formation (Permian) in southeastern Bighorn Basin, Wyoming. *AAPG Bulletin*, *46*(4), 478-503.

Calemma, V.; Iwanski, P.; Nali, M.; Scotti, R.; Montanari, L.; (1995). Structural Characterization of Asphaltenes of Different Origins. Energy & Fuels, 9, 225-230.

Chappaz, A., Lyons, T. W., Gregory, D. D., Reinhard, C. T., Gill, B. C., Li, C., & Large, R. R. (2014). Does pyrite act as an important host for molybdenum in modern and ancient euxinic sediments?. Geochimica et Cosmochimica Acta, 126, 112-122.

Chen, X., Ling, H. F., Vance, D., Shields-Zhou, G. A., Zhu, M., Poulton, S. W., & Archer, C. (2015). Rise to modern levels of ocean oxygenation coincided with the Cambrian radiation of animals. Nature communications, 6.

Chung, H. M., Brand, S. W., & Grizzle, P. L. (1981). Carbon isotope geochemistry of Paleozoic oils from Big Horn Basin. Geochimica et Cosmochimica Acta, 45(10), 1803-1815.

Claypool, G. E., Love, A. H., & Maughan, E. K. (1978). Organic geochemistry, incipient metamorphism, and oil generation in black shale members of Phosphoria Formation, western interior United States. *AAPG Bulletin*, *62*(1), 98-120.

Clayton, C. J. (1991). Effect of maturity on carbon isotope ratios of oils and condensates. Organic Geochemistry, 17(6), 887-899.

Connan, J., & Lacrampe-Couloume, G. (1993). The origin of the Lacq superieur heavy oil accumulation and the giant Lacq inferieur gas field. Applied Petroleum Geochemistry, 3, 464-488.

Dahl, T. W., Canfield, D. E., Rosing, M. T., Frei, R. E., Gordon, G. W., Knoll, A. H., & Anbar, A. D. (2011). Molybdenum evidence for expansive sulfidic water masses in~ 750Ma oceans. Earth and Planetary Science Letters,311(3), 264-274.

Dahl, T. W., Ruhl, M., Hammarlund, E. U., Canfield, D. E., Rosing, M. T., & Bjerrum, C. J. (2013). Tracing euxinia by molybdenum concentrations in sediments using handheld X-ray fluorescence spectroscopy (HHXRF). Chemical Geology, 360, 241-251.

Dahl, T. W., Chappaz, A., Hoek, J., McKenzie, C. J., Svane, S., & Canfield, D. E. (2017). Evidence of molybdenum association with particulate organic matter under sulfidic conditions. Geobiology, 15(2), 311-323.

Dembicki Jr, H. (2009). Three common source rock evaluation errors made by geologists during prospect or play appraisals. AAPG bulletin, 93(3), 341-356.

Dewakar, Mishra, K. N., Chandra, K., Arunachalam, J., & Karunasagar, D. (2000). Isotopic fractionation of Ni 60/Ni 61 in kerogen and bitumen samples. Current Science, 1720-1723.

DiMarzio, J. M., Georgiev, S. V., Stein, H. J., Hannah, J. L. (2018). Residency of rhenium and osmium in a heavy crude oil. Geochimica et Cosmochimica Acta, 220, 180-200.

Dunk, R. M., Mills, R. A., & Jenkins, W. J. (2002). A reevaluation of the oceanic uranium budget for the Holocene. Chemical Geology, 190(1), 45-67.

Duyck, C., Miekeley, N., da Silveira, C. L. P., & Szatmari, P. (2002). Trace element determination in crude oil and its fractions by inductively coupled plasma mass spectrometry using ultrasonic nebulization of toluene solutions.*Spectrochimica Acta Part B: Atomic Spectroscopy*, *57*(12), 1979-1990.

Elrick, M., Polyak, V., Algeo, T. J., Romaniello, S., Asmerom, Y., Herrmann, A. D., ... & Chen, Z. Q. (2017). Global-ocean redox variation during the middle-late Permian through Early Triassic based on uranium isotope and Th/U trends of marine carbonates. Geology, 45(2), 163-166.

Erickson, B. E., & Helz, G. R. (2000). Molybdenum (VI) speciation in sulfidic waters: stability and lability of thiomolybdates. Geochimica et Cosmochimica Acta, 64(7), 1149-1158.

Filby, R. H. (1994). Origin and nature of trace element species in crude oils, bitumens and kerogens: implications for correlation and other geochemical studies. Geological Society, London, Special Publications, 78(1), 203-219.

Filby, R.H., and Van Berkel, G.J., Geochemistry of Metal Complexes in Petroleum, Source Rocks and Coal: An Overview. In: Filby, R.H., and Branthaver, J.F. (Eds.), Metal Complexes in Fossil Fuels: Geochemistry, Characterization, and Processing. American Chemical Society, 1987, 344, 2-39.

Francois, R. (1988). A study on the regulation of the concentrations of some trace metals (Rb, Sr, Zn, Pb, Cu, V, Cr, Ni, Mn and Mo) in Saanich Inlet sediments, British Columbia, Canada. Marine geology, 83(1), 285-308.

Goldstein, T., & Aizenshtat, Z. (1994). Thermochemical sulfate reduction a review. Journal of Thermal Analysis and Calorimetry, 42(1), 241-290.

Goldberg, T., Archer, C., Vance, D., & Poulton, S. W. (2009). Mo isotope fractionation during adsorption to Fe (oxyhydr) oxides. Geochimica et Cosmochimica Acta, 73(21), 6502-6516.

Goldberg, T., Gordon, G., Izon, G., Archer, C., Pearce, C. R., McManus, J., ... & Rehkämper, M. (2013). Resolution of inter-laboratory discrepancies in Mo isotope data: an intercalibration. Journal of Analytical Atomic Spectrometry, 28(5), 724-735.

Goldhaber, M. B., & Orr, W. L. (1995). Kinetic controls on thermochemical sulfate reduction as a source of sedimentary H_2S.

Gradstein, F. M., Ogg, J. G., Smith, A. G., Bleeker, W., & Lourens, L. J. (2004). A new geologic time scale, with special reference to Precambrian and Neogene. Episodes, 27(2), 83-100.

Helz, G. R., Bura-Nakić, E., Mikac, N., & Ciglenečki, I. (2011). New model for molybdenum behavior in euxinic waters. Chemical Geology, 284(3), 323-332.

Herrmann, A. D., Kendall, B., Algeo, T. J., Gordon, G. W., Wasylenki, L. E., & Anbar, A. D. (2012). Anomalous molybdenum isotope trends in Upper Pennsylvanian euxinic facies: Significance for use of δ 98 Mo as a global marine redox proxy. Chemical Geology, 324, 87-98.

Hiatt, E. E., & Budd, D. A. (2003). Extreme paleoceanographic conditions in a Paleozoic oceanic upwelling system: organic productivity and widespread phosphogenesis in the Permian Phosphoria Sea. SPECIAL PAPERS-GEOLOGICAL SOCIETY OF AMERICA, 245-264.

Kato, Y., Nakao, K., & Isozaki, Y. (2002). Geochemistry of Late Permian to Early Triassic pelagic cherts from southwest Japan: implications for an oceanic redox change. Chemical Geology, 182(1), 15-34.

Karchmer, J. H., & Gunn, E. L. (1952). Determination of trace metals in petroleum fractions. Analytical chemistry, 24(11), 1733-1741.

Kendall, B., Creaser, R. A., Gordon, G. W., & Anbar, A. D. (2009a). Re–Os and Mo isotope systematics of black shales from the Middle Proterozoic Velkerri and Wollogorang formations, McArthur Basin, northern Australia.Geochimica et Cosmochimica Acta, 73(9), 2534-2558.

Kendall, B., Creaser, R. A., & Selby, D. (2009b). 187Re-187Os geochronology of Precambrian organic-rich sedimentary rocks. Geological Society, London, Special Publications, 326(1), 85-107.

Kendall, B., Gordon, G. W., Poulton, S. W., & Anbar, A. D. (2011). Molybdenum isotope constraints on the extent of late Paleoproterozoic ocean euxinia. Earth and Planetary Science Letters, 307(3), 450-460.

Kendall, B., Komiya, T., Lyons, T. W., Bates, S. M., Gordon, G. W., Romaniello, S. J., ... & Sawaki, Y. (2015). Uranium and molybdenum isotope evidence for an episode of widespread ocean oxygenation during the late Ediacaran Period. Geochimica et Cosmochimica Acta, 156, 173-193.

Kendall, B., Dahl, T. W., & Anbar, A. D. (2017). The stable isotope geochemistry of molybdenum. Reviews in Mineralogy and Geochemistry, 82(1), 683-732.

King, E. K., Thompson, A., Chadwick, O. A., & Pett-Ridge, J. C. (2016). Molybdenum sources and isotopic composition during early stages of pedogenesis along a basaltic climate transect. Chemical Geology, 445, 54-67.

Kirschbaum, M. A., Lillis, P. G., & Roberts, L. N. R. (2007). Geologic assessment of undiscovered oil and gas resources in the Phosphoria total petroleum system of the Wind River Basin Province, Wyoming. Petroleum Systems and Geologic Assessment of Oil and Gas in the Wind River Basin Province, Wyoming.

Kuo, L. C. (1994). An experimental study of crude oil alteration in reservoir rocks by water washing. *Organic Geochemistry*, *21*(5), 465-479.

Larson, P. B., Maher, K., Ramos, F. C., Chang, Z., Gaspar, M., & Meinert, L. D. (2003). Copper isotope ratios in magmatic and hydrothermal ore-forming environments. *Chemical Geology*, 201(3), 337-350.

Lau, K. V., Maher, K., Altiner, D., Kelley, B. M., Kump, L. R., Lehrmann, D. J., ... & Payne, J. L. (2016). Marine anoxia and delayed Earth system recovery after the end-Permian extinction. Proceedings of the National Academy of Sciences, 113(9), 2360-2365.

Lehrmann, D. J., Payne, J. L., Felix, S. V., Dillett, P. M., Wang, H., Yu, Y., & Wei, J. (2003). Permian–Triassic boundary sections from shallow-marine carbonate platforms of the Nanpanjiang Basin, South China: implications for oceanic conditions associated with the end-Permian extinction and its aftermath. Palaios, 18(2), 138-152.

Lewan, M. D., & Maynard, J. B. (1982). Factors controlling enrichment of vanadium and nickel in the bitumen of organic sedimentary rocks. Geochimica et Cosmochimica Acta, 46(12), 2547-2560.

Lillis, P. G., & Selby, D. (2013). Evaluation of the rhenium–osmium geochronometer in the Phosphoria petroleum system, Bighorn Basin of Wyoming and Montana, USA. *Geochimica et Cosmochimica Acta*, *118*, 312-330.

Lyons, T. W., Anbar, A. D., Severmann, S., Scott, C., & Gill, B. C. (2009). Tracking euxinia in the ancient ocean: a multiproxy perspective and Proterozoic case study. *Annual Review of Earth and Planetary Sciences*, *37*, 507-534.

Lyons, T. W., Werne, J. P., Hollander, D. J., & Murray, R. W. (2003). Contrasting sulfur geochemistry and Fe/Al and Mo/Al ratios across the last oxic-to-anoxic transition in the Cariaco Basin, Venezuela. *Chemical Geology*,*195*(1), 131-157.

Lyons, T. W., Reinhard, C. T., & Planavsky, N. J. (2014). The rise of oxygen in Earth/'s early ocean and atmosphere. Nature, 506(7488), 307-315.

Machel, H. G., Krouse, H. R., & Sassen, R. (1995). Products and distinguishing criteria of bacterial and thermochemical sulfate reduction. Applied geochemistry, 10(4), 373-389.

Machel, H. G. (2001). Bacterial and thermochemical sulfate reduction in diagenetic settings—old and new insights. *Sedimentary Geology*, *140*(1), 143-175.

Marcano, N., Larter, S., & Mayer, B. (2013). The impact of severe biodegradation on the molecular and stable (C, H, N, S) isotopic compositions of oils in the Alberta Basin, Canada. *Organic geochemistry*, *59*, 114-132.

Manning, D. A., & Gize, A. P. (1993). The role of organic matter in ore transport processes. In Organic Geochemistry (pp. 547-563). Springer US.

Maughan, E. K. (1975). Organic carbon in shale beds of the Permian Phosphoria Formation of eastern Idaho and adjacent states—a summary report.

Maughan, E. K. (1994). Phosphoria Formation (Permian) and its resource significance in the Western Interior, USA.

Marcano, N., Larter, S., & Mayer, B. (2013). The impact of severe biodegradation on the molecular and stable (C, H, N, S) isotopic compositions of oils in the Alberta Basin, Canada. *Organic geochemistry*, *59*, 114-132.

Mason, T. F., Weiss, D. J., Chapman, J. B., Wilkinson, J. J., Tessalina, S. G., Spiro, B., ... & Coles, B. J. (2005). Zn and Cu isotopic variability in the Alexandrinka volcanic-hosted massive sulphide (VHMS) ore deposit, Urals, Russia. Chemical Geology, 221(3), 170-187.

McKelvey, V. E., Williams, J. S., Sheldon, R. P., Cressman, E. R., Cheney, T. M., & Swanson, R. W. (1956). Summary description of Phosphoria, Park City, and Shedhorn formations in western phosphate Field. AAPG Bulletin,40(12), 2826-2863.

McLennan, S. M., & Taylor, S. R. (1991). Sedimentary rocks and crustal evolution: tectonic setting and secular trends. The Journal of Geology, 99(1), 1-21.

McLennan, S. M. (2001). Relationships between the trace element composition of sedimentary rocks and upper continental crust. Geochemistry, Geophysics, Geosystems, 2(4).

Morse, J. W., & Luther, G. W. (1999). Chemical influences on trace metal-sulfide interactions in anoxic sediments. Geochimica et Cosmochimica Acta, 63(19), 3373-3378.

Moynier, F., Vance, D., Fujii, T., & Savage, P (2017). The stable isotope geochemistry of Zinc and Copper. Reviews in Mineralogy and Geochemistry, 82(1), 543-600.

Miller, C. A., Peucker-Ehrenbrink, B., Walker, B. D., & Marcantonio, F. (2011). Re-assessing the surface cycling of molybdenum and rhenium. Geochimica et Cosmochimica Acta, 75(22), 7146-7179.

Murgich, J.; Rodríguez, J. M.; Aray, Y.; (1999). Molecular Recognition and Molecular Mechanics of Micelles of Some Model Asphaltenes and Resins. Energy & Fuels, 10, 68-76.

Nägler, T. F., Anbar, A. D., Archer, C., Goldberg, T., Gordon, G. W., Greber, N. D., ... & Vance, D. (2014). Proposal for an international molybdenum isotope measurement standard and data representation. Geostandards and Geoanalytical Research, 38(2), 149-151.

Nägler, T. F., Neubert, N., Böttcher, M. E., Dellwig, O., & Schnetger, B. (2011). Molybdenum isotope fractionation in pelagic euxinia: Evidence from the modern Black and Baltic Seas. Chemical Geology, 289(1), 1-11.

Nägler, T. F., Siebert, C., Lüschen, H., & Böttcher, M. E. (2005). Sedimentary Mo isotope record across the Holocene fresh–brackish water transition of the Black Sea. Chemical Geology, 219(1), 283-295.

Nakagawa, Y., Takano, S., Firdaus, M. L., Norisuye, K., Hirata, T., Vance, D., & Sohrin, Y. (2012). The molybdenum isotopic composition of the modern ocean. Geochemical Journal, 46(2), 131-141.

Neubert, N., Nägler, T. F., & Böttcher, M. E. (2008). Sulfidity controls molybdenum isotope fractionation into euxinic sediments: Evidence from the modern Black Sea. *Geology*, *36*(10), 775-778.

Neely, R. A., Gislason, S. R., Ólafsson, M., McCoy-West, A. J., Pearce, C. R., & Burton, K. W. (2018). Molybdenum isotope behaviour in groundwaters and terrestrial hydrothermal systems, Iceland. Earth and Planetary Science Letters, 486, 108-118.

Nordgard Erland L., Sørland Geir, And Sjoblom Johan, (2009). Behavior of Asphaltene Model Compounds at W/O Interfaces. Langmuir Article 2010, 26(4), 2352–2360.

Noordmann, J., Weyer, S., Montoya-Pino, C., Dellwig, O., Neubert, N., Eckert, S., ... and Böttcher, M. E. (2015). Uranium and molybdenum isotope systematics in modern euxinic basins: Case studies from the central Baltic Sea and the Kyllaren fjord (Norway). Chemical Geology, 396, 182-195.

Noordmann, J., Weyer, S., Georg, R. B., Jöns, S., and Sharma, M. (2016). 238U/235U isotope ratios of crustal material, rivers and products of hydrothermal alteration: new insights on the

oceanic U isotope mass balance. Isotopes in environmental and health studies, 52(1-2), 141-163.

Odin, G. S., & Letolle, R. (1980). Glauconitization and Phosphatization Environments a Tentative Comparison, in: Marine phosphorites; geochemistry, occurrence, genesis, Y. K. Bentor ed., Society of Economic Paleontologists and Mineralogists Special Publication 29, p. 227-237.

Orr, W. L. (1974). Changes in sulfur content and isotopic ratios of sulfur during petroleum maturation--study of Big Horn basin Paleozoic oils. *AAPG bulletin*, *58*(11), 2295-2318.

Orr, W. L. (1986). Kerogen/asphaltene/sulfur relationships in sulfur-rich Monterey oils. Organic geochemistry, 10(1-3), 499-516.

Partin, C. A., Bekker, A., Planavsky, N. J., Scott, C. T., Gill, B. C., Li, C., ... & Love, G. D. (2013). Large-scale fluctuations in Precambrian atmospheric and oceanic oxygen levels from the record of U in shales. Earth and Planetary Science Letters, 369, 284-293.

Parrish, J. T. (1982). Upwelling and petroleum source beds, with reference to Paleozoic. AAPG Bulletin, 66(6), 750-774.

Peters, K. E., Walters, C. C., & Moldowan, J. M. (2005). *The biomarker guide: biomarkers and isotopes in the environment and human history* (Vol. 1). Cambridge University Press.

Philp, R. P. (2004). Formation and geochemistry of oil and gas. *Treatise on Geochemistry*, *7*, 223-256.

Piper, D. Z., & Link, P. K. (2002). An upwelling model for the Phosphoria sea: A Permian, ocean-margin sea in the northwest United States. AAPG bulletin, 86(7)

Poulson, R. L., Siebert, C., McManus, J., & Berelson, W. M. (2006). Authigenic molybdenum isotope signatures in marine sediments. *Geology*, *34*(8), 617-620.

Proemse, B. C., Grasby, S. E., Wieser, M. E., Mayer, B., & Beauchamp, B. (2013) Molybdenum isotopic evidence for oxic marine conditions during the latest Permian extinction. *Geology, 41(9)*, 967-970.

Reinhard, C. T., Planavsky, N. J., Robbins, L. J., Partin, C. A., Gill, B. C., Lalonde, S. V., Bekker, A., Konhauser, K.O. and Lyons, T. W. (2013). Proterozoic ocean redox and biogeochemical stasis. Proceedings of the National Academy of Sciences, 110(14), 5357-5362.

Roberts, L. N., Finn, T. M., Lewan, M. D., & Kirschbaum, M. A. (2008). Burial history, thermal maturity, and oil and gas generation history of petroleum systems in the Bighorn Bsin, Wyoming and Montana. U.S. Geological Survey Scientific Investigations Report 2008-5037. 28p.

Romaniello, S. J., Herrmann, A. D., & Anbar, A. D. (2016). Syndepositional diagenetic control of molybdenum isotope variations in carbonate sediments from the Bahamas. Chemical Geology, 438, 84-90.

Rogel, E.J.; (2000). Simulation of Interactions in Asphaltenes Aggregates. Energy & Fuels, 14, 566-574

Ruebsam, W., Dickson, A. J., Hoyer, E. M., & Schwark, L. (2017). Multiproxy reconstruction of oceanographic conditions in the southern epeiric Kupferschiefer Sea (Late Permian) based on redox-sensitive trace elements, molybdenum isotopes and biomarkers. Gondwana Research, 44, 205-218.

Sahoo, S. K., Planavsky, N. J., Jiang, G., Kendall, B., Owens, J. D., Wang, X., ... & Lyons, T. W. (2016). Oceanic oxygenation events in the anoxic Ediacaran ocean. Geobiology, 14(5), 457-468.

Sageman, B. B., & Lyons, T. W. (2003). Geochemistry of fine-grained sediments and sedimentary rocks. Treatise on geochemistry, 7, 115-158.

Scholz, F., Siebert, C., Dale, A. W., & Frank, M. (2017). Intense molybdenum accumulation in sediments underneath a nitrogenous water column and implications for the reconstruction of paleo-redox conditions based on molybdenum isotopes. Geochimica et Cosmochimica Acta, 213, 400-417.

Scott, C., & Lyons, T. W. (2012). Contrasting molybdenum cycling and isotopic properties in euxinic versus non-euxinic sediments and sedimentary rocks: refining the paleoproxies. *Chemical Geology*, *324*, 19-27.

Scott, C., Slack, J. F., & Kelley, K. D. (2017). The hyper-enrichment of V and Zn in black shales of the Late Devonian-Early Mississippian Bakken Formation (USA). Chemical Geology, 452, 24-33.

Selby, D., Creaser, R. A., & Fowler, M. G. (2007). Re–Os elemental and isotopic systematics in crude oils. Geochimica et Cosmochimica Acta, 71(2), 378-386.

Siebert, C., Nägler, T. F., von Blanckenburg, F., & Kramers, J. D. (2003). Molybdenum isotope records as a potential new proxy for paleoceanography.*Earth and Planetary Science Letters*, *211*(1), 159-171.

Stirling, C. H., Andersen, M. B., Potter, E. K., and Halliday, A. N. (2007). Low temperature isotopic fractionation of uranium. Earth and Planetary Science Letters, 264(1), 208-225.

Siebert, C., McManus, J., Bice, A., Poulson, R., & Berelson, W. M. (2006). Molybdenum isotope signatures in continental margin marine sediments.*Earth and Planetary Science Letters*, *241*(3), 723-733.

Speight, J. G.; Long R.B., (1995). The concept of asphaltene revisited. AICHE: Spring National Meeting Preprint, 78a.

Speight, J. G. (1994). Chemical and physical studies of petroleum asphaltenes. In Developments in petroleum science (Vol. 40, pp. 7-65). Elsevier.

Swainson, I. P. (2017). *Reviews in Mineralogy & Geochemistry*.

Takahashi, S., Yamasaki, S. I., Ogawa, Y., Kimura, K., Kaiho, K., Yoshida, T., & Tsuchiya, N. (2014). Bioessential element-depleted ocean following the euxinic maximum of the end-Permian mass extinction. Earth and Planetary Science Letters, 393, 94-104.

Thomas, L. E. (1965). Sedimentation and structural development of Big Horn basin. *AAPG Bulletin*, *49*(11), 1867-1877.

Tissot, B., & Welte, D. (2012). Petroleum formation and occurrence: a new approach to oil and gas exploration. Springer Science & Business Media.

Tribovillard, N., Algeo, T. J., Lyons, T., & Riboulleau, A. (2006). Trace metals as paleoredox and paleoproductivity proxies: an update. *Chemical geology*,*232*(1), 12-32.

Trejo, F., Ancheyta J., (2007). Characterization of Asphaltene Fractions from Hydrotreated Maya Crude Oil. Ind. Eng. Chem. Res., 46, 7571-7579.

ULMER-SCHOLLE, D. S., & Scholle, P. A. (1994). Replacement of evaporites within the Permian Park City Formation, Bighorn Basin, Wyoming, USA. Sedimentology, 41(6), 1203-1222.

Ventura, G. T., Gall, L., Siebert, C., Prytulak, J., Szatmari, P., Hürlimann, M., & Halliday, A. N. (2015). The stable isotope composition of vanadium, nickel, and molybdenum in crude oils. *Applied Geochemistry*, *59*, 104-117.

Voegelin, A. R., Nägler, T. F., Samankassou, E., & Villa, I. M. (2009). Molybdenum isotopic composition of modern and Carboniferous carbonates. Chemical Geology, 265(3), 488-498.

Wagner, M., Chappaz, A., & Lyons, T. W. (2017). Molybdenum speciation and burial pathway in weakly sulfidic environments: Insights from XAFS. Geochimica et Cosmochimica Acta, 206, 18-29.

Walling, C. T. (2010). Stratigraphy and provenance of mudstone in the Phosphoria Formation (Vol. 72, No. 05).

Wardlaw, B. R., & Collinson, J. W. (1986). Paleontology and deposition of the Phosphoria Formation. Rocky Mountain Geology, 24(2), 107-142.

Weyer S., Anbar A. D., Gerdes A., Gordon G. W., Algeo T. J. and Boyle E. A. (2008) Natural fractionation of $^{238}U/^{235}U$. Geochim. Cosmochim. Acta 72, 345–359.

Wignall, P. B., & Twitchett, R. J. (1996). Oceanic anoxia and the end Permian mass extinction. Science, 272(5265), 1155.

Wignall, P. B., Bond, D. P., Kuwahara, K., Kakuwa, Y., Newton, R. J., & Poulton, S. W. (2010). An 80 million year oceanic redox history from Permian to Jurassic pelagic sediments of the Mino-Tamba terrane, SW Japan, and the origin of four mass extinctions. Global and Planetary Change, 71(1), 109-123.

Worden, R. H., & Heasley, E. C. (2000). Effects of petroleum emplacement on cementation in carbonate reservoirs. Bulletin de la Societe geologique de France, 171(6), 607-620.

Worden, R. H., Smalley, P. C., & Oxtoby, N. H. (1995). Gas souring by thermochemical sulfate reduction at 140 C. *AAPG Bulletin*, *79*(6), 854-863.

Wu, F., Qi, Y., Yu, H., Tian, S., Hou, Z., & Huang, F. (2016). Vanadium isotope measurement by MC-ICP-MS. Chemical Geology, 421, 17-25.

Yarranton, H. W.; Hussein, H.; Masliyah, J. H.; (2000). Water-in-Hydrocarbon Stabilized by Asphaltenes at Low Concentrations. Journal of Colloid and Interface Science, 228, 52-63.

Yen, T.F. (1975) The Role of Trace Metals in Petroleum, Ann Arbor Science Publishers Inc., Ann Arbor, Michigan.

Zhang, F., Romaniello, S. J., Algeo, T. J., Lau, K. V., Clapham, M. E., Richoz, S., ... & Anbar, A. D. (2018). Multiple episodes of extensive marine anoxia linked to global warming and continental weathering following the latest Permian mass extinction. Science advances, 4(4), e1602921.

Zheng, Y., Anderson, R. F., van Geen, A., & Kuwabara, J. (2000). Authigenic molybdenum formation in marine sediments: a link to pore water sulfide in the Santa Barbara Basin. Geochimica et Cosmochimica Acta, 64(24), 4165-4178.

Zhou, L., Su, J., Huang, J., Yan, J., Xie, X., Gao, S., & Dai, M. (2011). A new paleoenvironmental index for anoxic events--Mo isotopes in black shales from Upper Yangtze marine sediments. Science China. Earth Sciences, 54(7), 1024.

Zhou, L., Wignall, P. B., Su, J., Feng, Q., Xie, S., Zhao, L., & Huang, J. (2012). U/Mo ratios and δ 98/95 Mo as local and global redox proxies during mass extinction events. Chemical Geology, 324, 99-107.

Zhu, C. Developing the Analytical Method for Molybdenum Isotope Analysis of Crude Oil. Thesis paper presented to the University of Waterloo.